



# Light Scalars in the Extended Georgi-Machacek Model

Poulami Mondal \* and Subrata Samanta †

*Department of Physics, Indian Institute of Technology Kanpur, Kanpur 208016, India*

(Dated: June 10, 2025)

## Abstract

We perform global fits of the charge-parity (CP)-conserving Georgi-Machacek (GM) and extended Georgi-Machacek (eGM) models, incorporating a light CP-even beyond the Standard Model (BSM) scalar within the mass range of 90 GeV to 100 GeV. These fits combine the Higgs signal strengths and direct search limits from ATLAS and CMS at  $\sqrt{s} = 8$  and 13 TeV,  $B$ -physics observables, and theoretical constraints arising from next-to-leading order (NLO) unitarity and bounded-from-below (BFB) conditions on the scalar potential. The presence of a light BSM scalar significantly tightens the upper bounds on the masses and mass differences of the remaining BSM scalars due to NLO unitarity and BFB constraints. From the global fit, we show that the LHC diphoton and LEP  $b\bar{b}$  excesses around 95 GeV are well compatible with the observed 125 GeV Higgs data. Whereas the CMS ditau excess is incompatible with the 125 GeV Higgs signal strength data in both the CP-conserving GM and eGM models. We present the results from the combined fit, including the 95 GeV Higgs signal strength data. In the eGM model, the triplet VEV cannot exceed 12 GeV for additional BSM scalar masses below 160 GeV and approximately 25 GeV for additional BSM scalar masses above 160 GeV. The masses of additional BSM scalars cannot exceed 600 GeV. The maximum mass splitting is of around 120 GeV within the members of each custodial multiplet, and up to 250 GeV between the members of different multiplets. In the GM model, these constraints become more stringent: the triplet VEV is limited to below 15 GeV if the additional BSM scalar masses are above 160 GeV, which tightens to 4 GeV once the BSM scalar masses are below 160 GeV. Masses of the quintet  $m_5$  and the triplet  $m_3$  are restricted to be below 530 GeV and 320 GeV, respectively. A mass hierarchy,  $m_5 > m_3$ , is favoured in the high-mass region, with the mass splitting constrained to be less than 210 GeV.

Keywords: Beyond Standard Model, Higgs Physics, Multi-Higgs Models

---

\* [poulamim@iitk.ac.in](mailto:poulamim@iitk.ac.in)

† [samantaphy20@iitk.ac.in](mailto:samantaphy20@iitk.ac.in)

## I. INTRODUCTION

Despite the discovery of the Higgs boson with a mass around 125 GeV [1, 2] at the Large Hadron Collider (LHC), the underlying mechanism of electroweak symmetry breaking (EWSB) in the Standard Model (SM) remains elusive. Beyond the SM (BSM) particles with a higher representation of the  $SU(2)_L$  gauge group leave an imprint on the EWSB mechanism that can be detected via SM-like Higgs couplings to the vector bosons and fermions. Results from the latest ATLAS and CMS Run 2 data allow for a deviation within  $\sim 10\%$  in the SM-like Higgs coupling values from their SM prediction [3–21], leaving room for extended scalar sectors. The search for BSM scalars is a primary focus of the current LHC programme, offering key insights into the mechanism behind electroweak symmetry breaking.

Recent analyses by both the ATLAS and CMS collaborations at the LHC have reported intriguing hints of new resonances. For instance, the CMS collaboration has reported a new scalar resonance near 650 GeV, decaying to  $W^+W^-$  [22]. ATLAS has observed a hint of a doubly-charged scalar around 450 GeV decaying to same-sign  $W$  boson pairs [23]. Additionally, searches for Higgs bosons above 125 GeV have revealed several mild excesses involving both neutral and charged scalars [24–27]. In the ongoing search for a light Higgs boson, the CMS collaboration observed a diphoton resonance near 95.4 GeV with local significances of  $2.8\sigma$ , based on 8 TeV data [28] and the full Run 2 dataset at 13 TeV [29]. The updated CMS analysis of the full 13 TeV dataset ( $132.2\text{ fb}^{-1}$ ) strengthens this hint, reporting a  $2.9\sigma$  local excess at the same mass [30]. ATLAS reported a  $1.7\sigma$  local excess at the same mass [31] consistent with CMS. The Large Electron-Positron (LEP) collider also observed a local  $2.3\sigma$  excess near 95 GeV in the  $b\bar{b}$  channel [32, 33]. CMS has reported another excess in the  $\tau^+\tau^-$  channel around 100 GeV [34] well compatible with a mass of 95.4 GeV with  $2.6\sigma$  local significance.

The interpretation of the 95 GeV scalar excesses within the framework of extended scalar sector models has been the focus of numerous recent studies [35–80]. The two-Higgs Doublet Model (2HDM), a minimal such extension, has been widely studied to explain these excesses [35, 40, 45, 47, 48, 50, 55, 57, 58, 66, 69, 75, 79, 80]. To account for both the LEP and LHC excesses within the 2HDM, charge-parity (CP) conservation in the scalar potential must be relaxed [56]. However, the parameter space accommodating both the CMS diphoton and ditau excesses is in tension with flavour constraints, particularly from  $b \rightarrow s\gamma$  transitions [56]. Models with  $SU(2)_L$  scalar triplets feature a doubly-charged scalar that can enhance the loop-induced  $\gamma\gamma$  decay rate of CP-even scalars,<sup>1</sup> and explain the 95 GeV scalar excesses [51, 53, 59, 62, 63, 65, 73, 77, 78]. In addition to that, the scalar  $SU(2)_L$  triplet extensions of the SM have various other interesting phenomenological aspects at the LHC [81–113] and future colliders [114–123]. A minimal such CP-conserving triplet extension of the SM requires one complex triplet with hypercharge  $Y = 1$  and one real triplet with  $Y = 0$ , to keep the tree-level  $\rho$  parameter equal to one due to custodial symmetry (CS). The Georgi-Machacek (GM) model achieves this through a global  $SU(2)_L \otimes SU(2)_R$  symmetry [81, 82]. The extended GM (eGM) model [100], however, maintains CS without enforcing this global symmetry, leading to non-degenerate scalar masses within CS multiplets and a richer collider phenomenology [110]. The CP-conserving GM model can simultaneously accommodate both the ATLAS and CMS diphoton excesses, as well as the LEP excess in the  $b\bar{b}$  final state [63]. The model can also explain the CMS ditau excess, assuming the 95 GeV scalar is interpreted as a twin-peak resonance [62]. A global fit of the GM model was first performed in Ref. [96], and subsequently updated in Ref. [103]. In a recent study [110], we explored the GM model’s parameter space from a global fit to the latest LHC data on SM-like Higgs signal strengths, including next-

<sup>1</sup> Singly-charged scalars will also contribute, but the decay rate of a doubly-charged scalar is four times greater than that of a singly-charged scalar, assuming equal scalar couplings.

to-leading-order (NLO) unitarity bounds. These analyses considered all exotic scalar masses to be heavier than the observed 125 GeV Higgs. A similar fit of the CP-conserving eGM model was first performed in Ref. [110].

In this work, we aim to explore the eGM model parameter space that remains allowed by NLO unitarity and BFB conditions in the presence of a light CP-even BSM scalar with a mass between 90 and 100 GeV. We perform a global Bayesian fit to the recent measurements of SM-like Higgs signal strengths and to the direct search limits from heavy and light scalar searches at the LHC. Indirect limits from  $B$ -physics observables, as reported by HFLAV [124], are also included. The fit incorporates updated theoretical bounds like NLO unitarity and bounded-from-below (BFB) conditions. As a case study, we consider the 95 GeV Higgs signal strength data and assess whether the eGM model can enhance the diphoton decay rate sufficiently to account for the excesses observed by the LHC, while satisfying the NLO unitarity and BFB conditions, and also simultaneously incorporate the  $b\bar{b}$  excess reported by LEP. Additionally, we revisit the GM model and pose the same question. We investigate whether the GM model can incorporate the observed excesses while satisfying NLO unitarity and BFB conditions.

The fit shows that although  $B$ -physics observables constrain the triplet vacuum expectation value (VEV) in the low-mass region, the most stringent limits in this region come from LHC direct searches. In the presence of a light neutral BSM scalar, NLO unitarity bounds significantly tighten the upper limits on the masses of the remaining BSM scalars and their mass splittings. We present the results of the combined fit, incorporating the 95 GeV signal strength data. We show the constraints on the triplet VEV as a function of the BSM scalar masses, along with the allowed ranges for both the masses and mass splittings of the BSM scalars in each model. From the global fit, we show that the LHC diphoton and LEP  $b\bar{b}$  excesses around 95 GeV are well compatible with the observed 125 GeV Higgs data. Whereas the CMS ditau excess is incompatible with the 125 GeV Higgs signal strength data in both the CP-conserving GM and eGM models.

This paper is organised as follows: A brief overview of the models is presented in Section II. One-loop results of the  $B$ -physics observables are discussed in Section III. Higgs signal strength observables are discussed in Section IV. We also briefly discuss the 95 GeV excesses observed in collider experiments and analyse the possibility of accommodating these excesses within the GM and eGM models. We explain our global fit set-up and list all relevant constraints in Section V. The results from the global fits are presented in Section VI. We conclude in Section VII. In Appendix A, we list the direct search data on charged scalars searches from the LHC. In Appendix B, we study the compatibility of the 95 GeV Higgs data with the observed 125 GeV Higgs data. All the supplementary figures are placed in Appendix C.

## II. MODELS

We extend the scalar sector of the Standard Model by introducing a real triplet  $\xi$  with hypercharge  $Y = 0$  and a complex triplet  $\chi$  with  $Y = 1$ . The most general  $SU(2)_L \otimes U(1)_Y$  invariant scalar potential, following the notation of Ref. [110], is given by,

$$\begin{aligned}
V = & -m_\phi^2(\phi^\dagger\phi) - m_\xi^2(\xi^\dagger\xi) - m_\chi^2(\chi^\dagger\chi) + \mu_1(\chi^\dagger t_a \chi)\xi_a + \mu_2(\phi^\dagger \tau_a \phi)\xi_a \\
& + \mu_3\left[(\phi^T \epsilon \tau_a \phi)\tilde{\chi}_a + \text{h.c.}\right] + \lambda_\phi(\phi^\dagger\phi)^2 + \lambda_\xi(\xi^\dagger\xi)^2 + \lambda_\chi(\chi^\dagger\chi)^2 \\
& + \tilde{\lambda}_\chi|\tilde{\chi}^\dagger\chi|^2 + \lambda_{\phi\xi}(\phi^\dagger\phi)(\xi^\dagger\xi) + \lambda_{\phi\chi}(\phi^\dagger\phi)(\chi^\dagger\chi) + \lambda_{\chi\xi}(\chi^\dagger\chi)(\xi^\dagger\xi) \\
& + \kappa_1|\xi^\dagger\chi|^2 + \kappa_2(\phi^\dagger\tau_a\phi)(\chi^\dagger t_a\chi) + \kappa_3\left[(\phi^T \epsilon \tau_a \phi)(\chi^\dagger t_a \xi) + \text{h.c.}\right], \tag{1}
\end{aligned}$$

where  $\phi$  is the SM Higgs doublet with hypercharge  $Y = 1/2$ ,  $\xi$  and  $\chi$  are the real and complex triplet fields with  $Y = 0$  and  $Y = 1$ , respectively. After the EWSB,  $\phi$ ,  $\xi$ , and  $\chi$  acquire VEVs  $v_\phi/\sqrt{2}$ ,  $v_\xi$ , and  $v_\chi$ , respectively. At tree-level, the  $\rho$  parameter is given by,

$$\rho = \frac{v_\phi^2 + 4(v_\xi^2 + v_\chi^2)}{v_\phi^2 + 8v_\chi^2}, \quad \text{with} \quad v_\phi^2 + 4v_\xi^2 + 4v_\chi^2 = v^2 \approx (246 \text{ GeV})^2.$$

Maintaining  $\rho = 1$  at tree level requires  $v_\chi = v_\xi$ . Following [100], we ensure  $\rho = 1$  remains preserved by setting  $v_\chi = v_\xi$  and imposing four constraints, as outlined in Ref. [110],

$$m_\chi^2 = 2m_\xi^2, \quad \mu_2 = \sqrt{2}\mu_3, \quad \lambda_{\chi\xi} = 2\lambda_\chi - 4\lambda_\xi, \quad \kappa_2 = 4\lambda_{\phi\xi} - 2\lambda_{\phi\chi} + \sqrt{2}\kappa_3. \quad (2)$$

This choice leads to the extended Georgi-Machacek (eGM) model. In the eGM model, there are ten additional parameters beyond those in the SM. These include one triplet VEV  $v_\chi$  (or equivalently  $\tan\beta$ ), one mixing angle  $\alpha$ , two cubic parameters  $\mu_1, \mu_2$ , and six scalar masses ( $m_H, m_A, m_{H^+}, m_{F^0}, m_{F^+}, m_{F^{++}}$ ). The mixing angle  $\delta$ , which describes the mixing between the singly-charged scalars, can alternatively be traded for the mass of the pseudoscalar  $m_A$  [110]. The expressions of the physical masses, mixing angles, and  $\tan\beta$  are given in Ref. [110].

The scalar sector of the Georgi-Machacek (GM) model extends the SM by incorporating a bi-doublet and bi-triplet under a global  $SU(2)_L \otimes SU(2)_R$  symmetry. This framework preserves  $\rho = 1$  at tree-level. Like the eGM model, the GM model contains one pair of doubly-charged scalars, two pairs of singly-charged scalars, three CP-even neutral scalars, and one CP-odd neutral pseudoscalar. These states are classified into one fiveplet, one triplet, and two singlets according to their transformation properties under custodial  $SU(2)$ . In the GM model, all physical scalars within a given custodial multiplet are mass-degenerate. We follow the notation of Ref. [94]: the custodial fiveplet contains  $H_5^{\pm\pm}$ ,  $H_5^\pm$ , and  $H_5^0$ ; the triplet includes  $H_3^\pm$ ,  $H_3^0$ ; and the two custodial singlets are  $H$  and  $h$ . We denote the corresponding masses by  $m_5$ ,  $m_3$ ,  $m_1$ , and  $m_h$ , respectively, where,  $h$  is identified with the SM-like Higgs boson, and  $v_\Delta$  represents the VEV of the triplet fields.

### III. B-PHYSICS OBSERVABLES

In the absence of tree-level Flavour-Changing Neutral Current (FCNC) interactions, extended scalar sectors are constrained by loop-induced  $B$ -meson decays due to the presence of charged scalars [125–127]. In models such as the 2HDM and the GM model, the most relevant  $B$ -physics observable is the  $b \rightarrow s\gamma$  decay rate [93, 128]. Therefore, in this paper, we focus on  $B$ -physics constraints, primarily arising from the quark-level transition  $b \rightarrow s\gamma$ .

#### A. The Decays $B \rightarrow X_s\gamma$

Constraints on exotic charged scalars from the  $b \rightarrow s\gamma$  decay have been studied in [129, 130] with references therein for the 2HDM and in [93] for the GM model. Following [131, 132], we consider two physical observables that impose the strongest constraints on the  $b \rightarrow s\gamma$  amplitude: (i) the CP- and isospin- averaged branching ratio  $\mathcal{B}_{s\gamma}$  and (ii) the ratio,

$$R_\gamma \equiv \frac{\mathcal{B}_{(s+d)\gamma}}{\mathcal{B}_{c\ell\nu}}, \quad (3)$$

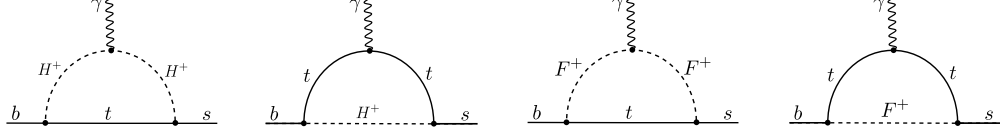


FIG. 1. One-particle irreducible (1PI) Feynman diagrams contributing to  $\Delta C_7$  and  $\Delta C_8$  at one-loop order in the eGM model.

where  $\mathcal{B}_{(s+d)\gamma}$  and  $\mathcal{B}_{cl\nu}$  are the inclusive branching ratios of the weak radiative and semileptonic decays. The current experimental average for  $\mathcal{B}_{s\gamma}$  and  $R_\gamma$  at  $E_0 = 1.6$  GeV reads [124, 133]

$$\mathcal{B}_{s\gamma}^{\text{exp}} = (3.49 \pm 0.19) \times 10^{-4}, \quad R_\gamma^{\text{exp}} = (3.22 \pm 0.15) \times 10^{-3}. \quad (4)$$

Theoretical analyses of rare  $B$ -meson decays are conducted within an effective theory framework, where all heavier SM and relevant BSM particles are decoupled. In the presence of charged scalar particles, new physics contributions to the  $b \rightarrow s\gamma$  transition are encoded in the Wilson coefficients  $\Delta C_7$  and  $\Delta C_8$ , which parameterise the new physics effects on the electromagnetic and chromomagnetic operators. Their most general expressions are given up to Next-to-Next-to-Leading Order (NNLO) QCD corrections for the SM [134–136] and for the 2HDM [129]. Extending these results to the eGM model, which features two charged scalar particles coupling to fermions, is straightforward. In this analysis, we consider the Leading Order (LO) contributions to the renormalised Wilson coefficients  $\Delta C_7$  and  $\Delta C_8$ , arising from loop diagrams involving charged bosons. The dominant contributions come from diagrams where charged bosons couple to the top quark, as illustrated in Figure 1. At the LO, the contributions of BSM charged scalars to the Wilson coefficients in the eGM model at the renormalisation scale  $\mu_0$  are given by,

$$\Delta C_{7,8}(\mu_0) = \frac{1}{3} t_\beta^2 c_\delta^2 F_{7,8}^{(1)}(y_1) - t_\beta^2 c_\delta^2 F_{7,8}^{(2)}(y_1) + \frac{1}{3} t_\beta^2 s_\delta^2 F_{7,8}^{(1)}(y_2) - t_\beta^2 s_\delta^2 F_{7,8}^{(2)}(y_2) \quad (5)$$

with

$$y_1 \equiv \frac{\bar{m}_t^2(\mu_0)}{m_{H^\pm}^2}, \quad y_2 \equiv \frac{\bar{m}_t^2(\mu_0)}{m_{F^\pm}^2}. \quad (6)$$

Here  $\bar{m}_t$  represents the  $\overline{MS}$  running mass, which is related to the pole mass  $m_t$  by the relation [137],

$$\bar{m}_t(m_t) = m_t \left[ 1 - \frac{4}{3} \frac{\alpha_s(m_t)}{\pi} \right], \quad (7)$$

and the notations  $t_\beta$ ,  $s_\delta$ ,  $c_\delta$  represent  $\tan \beta$ ,  $\sin \delta$ , and  $\cos \delta$ , respectively. The NLO  $t$ -quark running mass at the scale  $\mu_0$  [137] is given by,

$$\bar{m}_t(\mu_0) = \bar{m}_t(m_t) \left[ \frac{\alpha_s(\mu_0)}{\alpha_s(m_t)} \right]^{\frac{\gamma_0}{2\beta_0}} \left[ 1 + \frac{\alpha_s(m_t)}{4\pi} \frac{\gamma_0}{2\beta_0} \left( \frac{\gamma_1}{\gamma_0} - \frac{\beta_1}{\beta_0} \right) \left( \frac{\alpha_s(\mu_0)}{\alpha_s(m_t)} - 1 \right) \right], \quad (8)$$

$$\gamma_0 = 8, \quad \gamma_1 = \frac{404}{3} - \frac{40}{9} n_f, \quad \beta_0 = 11 - \frac{2}{3} n_f, \quad \beta_1 = 102 - \frac{38}{3} n_f, \quad (9)$$

where  $n_f$  denotes the effective number of quark flavours and the values of  $\alpha_s$ , at a generic scale  $\mu$

are computed using the NLO result from Ref. [137, 138],

$$\alpha_s(\mu) = \frac{\alpha_s(M_Z)}{r(\mu)} \left( 1 - \frac{\beta_1}{\beta_0} \frac{\alpha_s(M_Z)}{4\pi} \frac{\ln r(\mu)}{r(\mu)} \right), \quad r(\mu) = 1 - \beta_0 \frac{\alpha_s(M_Z)}{2\pi} \ln \frac{M_Z}{\mu}. \quad (10)$$

The form of  $F_{7,8}^{(1)}(y_i)$  and  $F_{7,8}^{(2)}(y_i)$  for  $i = 1, 2$  are given by [137, 139, 140],

$$\begin{aligned} F_7^{(1)}(y_i) &= \frac{y_i(7 - 5y_i - 8y_i^2)}{24(y_i - 1)^3} + \frac{y_i^2(3y_i - 2)}{4(y_i - 1)^4} \ln y_i, \\ F_8^{(1)}(y_i) &= \frac{y_i(2 + 5y_i - y_i^2)}{8(y_i - 1)^3} - \frac{3y_i^2}{4(y_i - 1)^4} \ln y_i, \\ F_7^{(2)}(y_i) &= \frac{y_i(3 - 5y_i)}{12(y_i - 1)^2} + \frac{y_i(3y_i - 2)}{6(y_i - 1)^3} \ln y_i, \\ F_8^{(2)}(y_i) &= \frac{y_i(3 - y_i)}{4(y_i - 1)^2} - \frac{y_i}{2(y_i - 1)^3} \ln y_i. \end{aligned} \quad (11)$$

Incorporating improved non-perturbative contributions [136], the updated SM predictions for  $\mathcal{B}_{s\gamma}$  and  $R_\gamma$ , as estimated in [130], are given by,

$$\mathcal{B}_{s\gamma}^{\text{SM}} = (3.40 \pm 0.17) \times 10^{-4}, \quad R_\gamma^{\text{SM}} = (3.35 \pm 0.16) \times 10^{-3}, \quad (12)$$

for  $E_0 = 1.6$  GeV. Thus, the effects of the additional contributions  $\Delta C_{7,8}$  as given in Eq. (5) must be small; otherwise, they would increase the discrepancy between theory and experiment. In this scenario,  $\mathcal{B}_{s\gamma}$  and  $R_\gamma$  can be determined using the following simple linearized expressions [130],

$$\begin{aligned} \mathcal{B}_{s\gamma} \times 10^4 &= (3.40 \pm 0.17) - 8.25\Delta C_7(\mu_0) - 2.10\Delta C_8(\mu_0), \\ R_\gamma \times 10^3 &= (3.35 \pm 0.16) - 8.08\Delta C_7(\mu_0) - 2.06\Delta C_8(\mu_0), \end{aligned} \quad (13)$$

where  $\mu_0 = 160$  GeV. The GM model contributions  $\Delta C_{7,8}$  are derived from Eq. (5) by setting  $\delta = 0$  and replacing  $m_{H^\pm}$  with  $m_3$ . Note that the GM model contributions have the same structure as those in the Type-I 2HDM [93]. The observables  $\mathcal{B}_{s\gamma}$  and  $R_\gamma$ , each impose an upper bound on the triplet VEV as a function of the charged scalar masses. In our numerical analysis in Section VI, we present the allowed regions in these planes for both the GM and eGM models.

## IV. HIGGS SIGNAL STRENGTH

### A. SM-like Higgs, $h$

The signal strength for the production of the SM-like Higgs boson  $h$  (where  $m_h = 125.09$  GeV) via production channel  $i$  and its decay to final state  $f$  is defined as,

$$\mu_i^f \equiv r_i \cdot \frac{r_f}{\sum_{f' \in \{ZZ, WW, Z\gamma, \gamma\gamma, \mu\mu, bb, \tau\tau\}} r_{f'} \cdot \mathcal{B}_{\text{SM}}(h \rightarrow f')},$$

where  $r_i$  and  $r_f$  are the ratios of the production cross-sections  $\sigma_i$ 's (where  $i \in \{ggF, b\bar{b}h, \text{VBF}, Wh, Zh, t\bar{t}h, th\}$ ) and the partial decay width  $\Gamma^f$ 's (where  $f \in \{ZZ, WW, \gamma\gamma, Z\gamma, \mu\mu, bb, \tau\tau\}$ ) to their corresponding SM values.  $\mathcal{B}(h \rightarrow f)$ 's are the decay branching fractions for final state  $f$ .

In the  $\kappa$ -framework [3], the modifiers for SM Higgs coupling to vector bosons and fermions at tree-level in both the GM and eGM models are given by,<sup>2</sup>

$$\kappa_V^h = s_\alpha c_\beta + \sqrt{\frac{8}{3}} c_\alpha s_\beta, \quad \text{and} \quad \kappa_f^h = \frac{s_\alpha}{c_\beta}, \quad (14)$$

The experimental input values of  $h$  signal strengths based on the latest ATLAS and CMS Run 2 data at a center-of-mass energy of 13 TeV are presented in Tables 5 and 6, of Ref. [110]. The combined ATLAS and CMS Run 1 measurements of  $h$  signal strengths are provided in Table 2 of [141].

## B. Light Higgs, $\Phi_{95}$

Previously, LEP and, more recently, both Run 1 and Run 2 of the LHC have reported local excesses with a mass of around 95 GeV [28–34, 142]. For a given final state  $f$ , the signal strength of the light Higgs boson with a mass around 95 GeV,  $\Phi_{95}$  is defined as,

$$\mu_i^f \equiv r_i \cdot \frac{r_f}{\sum_{f' \in \{ZZ, WW, Z\gamma, \gamma\gamma, \mu\mu, bb, \tau\tau\}} r_{f'} \cdot \mathcal{B}_{\text{SM}}(\Phi_{95} \rightarrow f')}.$$

Here,  $r_i$  and  $r_f$  represent the ratios of the production cross-sections and partial decay widths, respectively, normalized to their SM expectations for a Higgs boson with a mass of approximately 95 GeV.  $\mathcal{B}_{\text{SM}}(\Phi_{95} \rightarrow f')$  denotes the branching ratio of hypothetical SM Higgs boson  $\Phi_{95}$  decaying into the final state  $f'$ .

### 1. The CMS and ATLAS diphoton excess

Diphoton searches at the LHC are among the most promising avenues for detecting additional neutral Higgs bosons with masses below 125 GeV. In recent years, the CMS collaboration has conducted searches for light Higgs bosons decaying into two photons using LHC data at both 8 TeV [28] and 13 TeV [29]. By combining the 8 TeV Run 1 and 13 TeV Run 2 datasets, with integrated luminosities of  $19.7 \text{ fb}^{-1}$  and  $35.9 \text{ fb}^{-1}$ , respectively, the CMS collaboration observed a scalar resonance at a mass of 95.3 GeV. This resonance, produced via gluon fusion and decaying into diphotons, was detected with a local significance of  $2.8 \sigma$  [29]. The updated CMS analysis with full Run 2 dataset with an integrated luminosity of  $132 \text{ fb}^{-1}$  at 13 TeV, reported a local excess with a local significance of  $2.9 \sigma$  at a mass of 95.4 GeV in the diphotons final state [30]. The corresponding signal strengths  $\mu_i^{\gamma\gamma}$  for the production modes  $i \in \{ggF, \text{VBF}\}$  are listed in Table 1.<sup>3</sup> On the other hand, the recent ATLAS analysis based on the full Run 2 dataset with an integrated luminosity of  $140 \text{ fb}^{-1}$  at 13 TeV, reported an excess at 95.4 GeV in the diphoton final state with a local significance of  $1.7 \sigma$  at 95.4 GeV [31]. This diphoton excess can be described by a scalar resonance produced dominantly in gluon fusion production at a mass of 95.4 GeV with a signal strength given in Table 1.

<sup>2</sup> Here we consider the SM-like Higgs  $h$  as the heavy custodial singlet, while the mass of the other custodial singlet must be less than 125 GeV.

<sup>3</sup> Notably, the updated CMS results report a significantly lower signal strength compared to previous analyses, while the local significance of the excess and the mass range remain unchanged. For further details, see [56].



## 2. The CMS ditau excess

The CMS collaboration observed an excess over the expected background in light Higgs boson searches involving ditau final states, consistent with a mass of  $\sim 95$  GeV under the assumption of gluon fusion production [34]. The excess was most prominent at a mass hypothesis of 100 GeV, with local and global significances of  $3.1\sigma$  and  $2.7\sigma$ , respectively. It also remains consistent with a scalar resonance at 95.4 GeV, where the local and global significances are  $2.6\sigma$  and  $2.3\sigma$ , respectively. The corresponding signal strength  $\mu_i^{\tau\tau}$  is listed in Table 1. To date, ATLAS has not published a search in the ditau final state covering the mass range around 95 GeV.

## 3. LEP excess

The LEP reported a mild excess with a local significance of  $2.3\sigma$  in the  $e^+e^- \rightarrow Z(\Phi \rightarrow b\bar{b})$  searches [32, 33], compatible with a scalar resonance at 95.4 GeV. The corresponding signal strength,  $\mu_i^{bb}$ , is given in Table 1.

Signal strength	Value	Correlation matrix		$\mathcal{L}$ [fb $^{-1}$ ]	Detector	Source
$\mu_{\text{ggF}}^{\gamma\gamma}$	$0.47 \pm 0.20$	1	$-0.52$	132.0	CMS	[30]
$\mu_{\text{VBF}}^{\gamma\gamma}$	$0.06 \pm 0.70$	$-0.52$	1			
$\mu_{\text{pp}}^{\gamma\gamma}$	$0.18 \pm 0.10$			140.0	ATLAS	[57]
$\mu_{\text{pp}}^{\tau\tau}$	$1.23 \pm 0.55$			138.0	CMS	[34]
$\mu_{\text{ee}}^{bb}$	$0.117 \pm 0.057$			2.461	LEP	[32, 36]

TABLE 1. Signal strength results of 95 GeV Higgs boson measured by ATLAS, CMS, and LEP.

## 4. GM/eGM interpretation of the excesses at 95 GeV

Here, we investigate the possibility of a neutral BSM scalar state with a mass of approximately 95 GeV within the CP-conserving GM and eGM models, assessing its ability to explain the excesses reported by CMS, ATLAS, and LEP. Both models feature three CP-even and one CP-odd scalar states, with two of the CP-even states being custodial singlets. We first examine whether a CP-even scalar state at 95 GeV can account for these excesses. Since the diphoton excess is primarily produced via gluon fusion, we exclude the possibility that the non-custodial singlet is responsible for this excess, as it does not have any tree-level couplings to fermions in these models. Therefore, in both models, we identify the lightest custodial singlet ( $H$ ) as a new particle state with a mass of approximately 95 GeV,  $\Phi_{95} = H$ . The heavier custodial singlet ( $h$ ) corresponds to the SM-like Higgs boson with a mass of 125 GeV.

In the  $\kappa$ -framework [3], the modifiers for a hypothetical SM Higgs  $H$  coupling to vector bosons and fermions at tree-level in both the GM and eGM models are given by,

$$\kappa_V^H = c_\alpha c_\beta - \sqrt{\frac{8}{3}} s_\alpha s_\beta, \quad \text{and} \quad \kappa_f^H = \frac{c_\alpha}{c_\beta}, \quad (15)$$



From Eqs. (14) and (15), we obtain the following relations among the coupling modifiers:

$$\kappa_f^h \kappa_V^h + \kappa_f^H \kappa_V^H = 1. \quad (16)$$

Next, we investigate whether the CP-odd scalar state ( $\Phi_{95} = H_3^0$  or  $A$ ) could be the source of the observed excess in both the CP-conserving GM and eGM models. The LEP cross-section limits are derived from searches for scalar resonances produced via Higgsstrahlung, which requires the scalar to have a coupling to  $Z$  bosons. The interpretation of this excess as a CP-odd state in both models is disfavoured, because of the vanishing coupling to vector bosons at tree-level. Therefore, in this work, we exclude the CP-odd scalar state ( $H_3^0$  or  $A$ ) as a viable candidate for the 95 GeV mass resonance responsible for the observed excesses.

## V. FIT SET-UP AND CONSTRAINTS

### A. Fit set-up

To delineate the viable parameter space of the GM and eGM models, we perform a global analysis using the open-source code **HEPfit** [143]. This involves a Bayesian fit carried out with a Markov Chain Monte Carlo (MCMC) algorithm implemented through the **Bayesian Analysis Toolkit** (BAT) library [144].<sup>4</sup>

In this study, we identify the heaviest custodial singlet as the SM-like Higgs boson  $h$  with a fixed mass of  $m_h = 125.09$  GeV, and vary the lightest custodial singlet ( $H$ ) in the range  $m_H \in [90, 100]$  GeV. All other Standard Model parameters are fixed to their best-fit values as reported in Ref. [145]. In the case of the eGM model, we make observables for heavy scalar masses within the range:  $m_{F^0}, m_{F^{++}} \in [0.08, 1]$  TeV, and  $m_A \in [0.01, 1]$  TeV. Due to stringent direct search limits on low-mass charged scalars from LEP [146], we impose a lower bound of 80 GeV on the charged scalars in our analysis. We list the input parameters of the GM and the eGM models and their priors in Table 2. For further details on the implementation of the GM and eGM models in **HEPfit**, we refer the reader to Refs. [96, 110].

GM		eGM	
Parameters	Range	Parameters	Range
$v_\Delta$	: [0, 60] GeV	$v_\chi$	: [0, 60] GeV
$\alpha$	: $[-\pi/2, \pi/2]$	$\alpha, \delta$	: $[-\pi/2, \pi/2]$
$\lambda_3, \lambda_5$	: $[-4\pi, 4\pi]$	$\lambda_\chi$	: $[0, 4\pi]$
$m_1$	: [90, 100] GeV	$\tilde{\lambda}_\chi, \kappa_1, \kappa_3$	: $[-4\pi, 4\pi]$
$m_3, m_5$	: [80, 1000] GeV	$m_H$	: [90, 100] GeV
		$m_{H^\pm}, m_{F^\pm}$	: [80, 1000] GeV

TABLE 2. Priors on the input parameters of the GM and eGM models.

<sup>4</sup> In our previous work [110], we extensively examined the viability of the GM and eGM models within the heavy Higgs scenario, where all BSM scalars are heavier than the observed 125 GeV Higgs boson. The current study extends the parameter space to include the possibility where the BSM scalars are lighter than the 125 GeV Higgs.

## B. Theoretical constraints

From theoretical perspective, we incorporate the constraints given in Ref. [110] in our fits:

- The Higgs potential must satisfy stability bounds for all possible three field directions up to a scale of 1 TeV.<sup>5</sup>
- Yukawa and quartic couplings must remain perturbative, bounded by  $\sqrt{4\pi}$  and  $4\pi$ , respectively, up to a scale of 1 TeV. Their evolution is governed by two-loop renormalisation group equations.
- The  $S$ -matrix eigenvalues for  $2 \rightarrow 2$  scattering, including NLO corrections, must satisfy unitarity bounds at 1 TeV. We also require NLO corrections to be small relative to the LO eigenvalues.

## C. Experimental Constraints

The experimental constraints included in our analysis are:

- The branching ratio  $\mathcal{B}_{s\gamma}$  and the ratio  $R_\gamma$ .
- $h$  signal strengths from the latest ATLAS and CMS Run 2 data at a center-of-mass energy of 13 TeV [110] and ATLAS and CMS combination for Run 1 data [141].
- $H$  signal strengths given in Table 1.
- Total decay widths of  $h$  and  $t$ -quark given in Table 3.
- Direct search limits of the heavy and light BSM scalars at the LHC.<sup>6</sup>

Observable	Value	$\mathcal{L}$ [fb <sup>-1</sup> ]	Detector	Source
$\Gamma_h$	$3.20 \pm 2.05$ MeV	138.0	CMS	[17]
	$4.50 \pm 2.75$ MeV	139.0	ATLAS	[147]
$\Gamma_t$	$1.360 \pm 0.127$ GeV	19.7	CMS	[148]

TABLE 3. Total decay widths of SM Higgs boson and top quark.

In this work, we analyse the eGM model, incorporating constraints from direct searches for heavy and light BSM scalars at the LHC. Furthermore, we include the latest exclusion limits from direct searches for both heavy and light BSM scalars for the GM model, providing an updated comparison with previous fits [96]. These direct search constraints are implemented as follows:

1. For a given process,  $X \rightarrow \Phi \rightarrow Y$ , we compute the theoretical production cross-section of a scalar particle  $\Phi$  ( $= A, F^0, H^\pm, F^\pm, F^{\pm\pm}$ ), and multiply it by its branching fraction to a specific decay channel, i.e.  $(\sigma \cdot \mathcal{B})_{\text{th}} = \sigma_{\text{th}}(X \rightarrow \Phi) \times \mathcal{B}_{\text{th}}(\Phi \rightarrow Y)$ .

<sup>5</sup> In our analysis, stability bounds refer to the scalar potential being bounded from below. The bound from metastability is not considered and will be explored in future work.

<sup>6</sup> In the heavy scalar scenario, BSM scalars are assumed to be heavier than the observed 125 GeV scalar, while the light scalar scenario corresponds to the BSM scalars with masses below 125 GeV.

2. Following [141, 149], we define the ratio,

$$R_{\text{direct}} = \frac{(\sigma \cdot \mathcal{B})_{\text{th}}}{(\sigma \cdot \mathcal{B})_{\text{obs}}}, \quad (17)$$

where  $(\sigma \cdot \mathcal{B})_{\text{obs}}$  denotes the observed 95% confidence level (CL) exclusion limits on  $\sigma \cdot \mathcal{B}$ , as provided by experimental collaborations. To compare the theoretical prediction with these experimental bounds, we treat the ratio  $R_{\text{direct}}$  as Gaussian-distributed variables under the null hypothesis, with a mean of zero. The corresponding standard deviation for  $R_{\text{direct}}$  is chosen such that a value of 1 is excluded at the 95% CL.

Among the three neutral scalars, one CP-even state,  $h$ , is fixed at 125 GeV, while the mass of the other CP-even state, denoted  $m_H$  in the eGM model and  $m_1$  in the GM model, lies in the range [90, 100] GeV. The third neutral scalar, a CP-even state, is fermiophobic, while the CP-odd state is gauge-phobic in both models. The theoretical predictions of  $\sigma \cdot \mathcal{B}$  for neutral and singly-charged scalars are taken from the well-established (Aligned-) 2HDM [141, 149, 150] and rescaled to match the GM and eGM frameworks. For the doubly-charged scalar, the theoretical values of  $\sigma \cdot \mathcal{B}$  are already implemented in **HEPfit** for the GM model [96], and these results are equally applicable to the eGM model. A summary of the latest collider constraints on the production and decay of additional heavy neutral scalars is provided in Tables 6–11 of Ref. [150], while the corresponding data for heavy charged scalars are provided in the Appendix A.

The presence of light scalars can modify the (invisible) total decay widths of several well-measured SM particles, such as the Higgs boson and the top quark. For instance, if the masses of BSM neutral scalars,  $\Phi = H$  or  $A$  in the eGM model ( $\Phi = H$  or  $H_3^0$  in the GM model), are lighter than the SM-like Higgs  $h$ , the cascade decays  $h \rightarrow \Phi \Phi^* \rightarrow \Phi b \bar{b}$  can be important in the region with low triplet VEV ( $v_\chi$  in the eGM and  $v_\Delta$  in the GM models). Because the  $\Phi b \bar{b}$  coupling varies as,  $g_{\Phi b \bar{b}} \sim 1/v_\chi$  in the eGM model ( $g_{\Phi b \bar{b}} \sim 1/v_\Delta$  in the GM model). In the mass range where  $m_h \lesssim 2m_\Phi - \Gamma_\Phi$ , the partial decay width for the above three-body decays are given in [151]. Additionally, in the presence of a light singly-charged scalar  $H_3^+$  in the GM model, a top quark decay via  $t \rightarrow H_3^+ b$  can alter the branching fractions of final states containing SM particles. Consequently, these observables are crucial for constraining the parameter space of the eGM model, as both singly-charged scalars ( $H^+, F^+$ ) couple to fermions. In our analysis, we include the latest ATLAS and CMS upper limits on  $\mathcal{B}(t \rightarrow H^+ b)$  and  $\mathcal{B}(t \rightarrow F^+ b)$  for the eGM model, and  $\mathcal{B}(t \rightarrow H_3^+ b)$  for the GM model, where the charged scalars subsequently decay into one of the following channels:  $\tau^+ \nu$ ,  $c \bar{s}$ , and  $c \bar{b}$ , as reported in Tables 12 and 13 of Ref. [150]. The ATLAS and CMS searches for light doubly-charged scalars in the leptonic final state assume a 100% branching fraction (see Refs. [22, 152–154]), since in this case the decay to vector boson final states is suppressed. In the GM (eGM) model, the process,  $H_5^{++} \rightarrow \ell^+ \ell^+$  ( $F^{++} \rightarrow \ell^+ \ell^+$ ) proceeds exclusively through the lepton number-violating coupling between the lepton doublet and the Higgs triplet fields. As our analysis assumes a triplet VEV of  $\mathcal{O}(1)$ , current experimental constraints do not exclude any region of the parameter space in either model. As a result, we do not consider these searches involving a light doubly-charged scalar in our study. We incorporate searches for a light neutral scalar, decaying into two photons or two vector bosons in both models, as given in Tables 8 and 9 of Ref. [150]. We include searches for a light pseudoscalar state  $A$  in the eGM model ( $H_3^0$  in the GM model) decaying into a pair of leptons, as reported by the ATLAS and CMS collaborations, given in Table 3 of Ref. [150]. In the GM model, the pseudoscalar  $H_3^0$  and the singly-charged scalars  $H_3^\pm$  are mass-degenerate. Consequently, the lower bound on  $m_{H_3^0}$  is set by the LEP limit on  $m_{H_3^\pm}$ , i.e.  $m_3 = 80$  GeV. All theoretical and experimental datasets for  $\sigma \cdot \mathcal{B}$  used in this work are discrete and are linearly interpolated throughout the analysis.

## VI. RESULTS

In this section, we present the allowed parameter space, taking into account all theoretical constraints and the 95.4% probability regions from the combined fits to experimental data for both the GM and eGM models. For the theoretical constraints, we assume flat likelihoods, and the allowed regions represent 100% probability contours. The results are based on the prior ranges specified in Tables 2 for the GM and eGM models, unless stated otherwise.

In Figure 2, we examine the impact of the  $B$ -physics observables,  $\mathcal{B}_{s\gamma}$  and  $R_\gamma$ , on the parameter space of both the GM and eGM models.<sup>7</sup> In the GM model, only the singly-charged scalar from the custodial triplet contributes to these  $B$ -physics observables. Each of these observables imposes an upper bound on the triplet VEV,  $v_\Delta$ , as a function of the singly-charged scalar mass,  $m_3$ , as shown in the left panel of Figure 2. As discussed in Section III, both singly-charged scalars,  $H^+$  and  $F^+$  contribute to these  $B$ -physics observables in the eGM model. The middle (right) panel of Figure 2 presents the corresponding allowed parameter space in the  $m_{H^+}$  vs.  $v_\chi$  ( $m_{F^+}$  vs.  $v_\chi$ ) plane for the eGM model. In both models, we observe that the latest result from HFLAV [124] on  $\mathcal{B}_{s\gamma}$  imposes a dominant constraint on the triplet VEV. Therefore, from this point onward, we consider only  $\mathcal{B}_{s\gamma}$  when discussing  $B$ -physics constraints. As seen in Figure 2, the triplet VEV is tightly constrained in the lower mass region of the charged scalars. This is because significant corrections to the Wilson coefficients  $\Delta C_{7,8}$  arise in this region due to large values of  $\tan\beta$  (see Eq. (11)). To keep  $\Delta C_{7,8}$  small, and thus maintain  $\mathcal{B}_{s\gamma}$  within the experimental range specified in Eq. (4), smaller values of  $\tan\beta$  are necessary. This highlights the significance of  $B$ -physics constraints, particularly when the charged scalar masses are low. In the GM model, the inclusion of the latest limit on  $\mathcal{B}_{s\gamma}$  from HFLAV [124] slightly tightens the upper bound on  $v_\Delta$  compared to the results presented in Ref. [93].<sup>8</sup> The upper bound on  $v_\chi$  is less stringent for low  $m_{H^+}$  compared to the corresponding upper bound on  $v_\Delta$  for low  $m_3$ . However, for large  $m_{H^+}$ , the upper bounds on the triplet VEV become comparable in both models. This behaviour arises because, at low  $m_{H^+}$ , the contribution to  $\Delta C_{7,8}$  in the eGM model is maximized and matches that of the GM model when  $m_{H^+}$  and  $m_{F^+}$  are degenerate. When this mass degeneracy is lifted, the heavier  $m_{F^+}$  contributes less significantly to  $\Delta C_7$  and  $\Delta C_8$ , resulting in weaker constraints on  $v_\chi$ . Conversely, at large  $m_{H^+}$ , the contribution to  $\Delta C_{7,8}$  saturates and becomes identical in both models, leading to equivalent bounds on the triplet VEV. A similar trend is also observed in the  $m_{F^+}$  vs.  $v_\chi$  plane, as we define  $m_{F^+}$  to be the heavier and  $m_{H^+}$  the lighter charged scalar mass, with the possibility of eigenstate interchange depending on the parameter space.

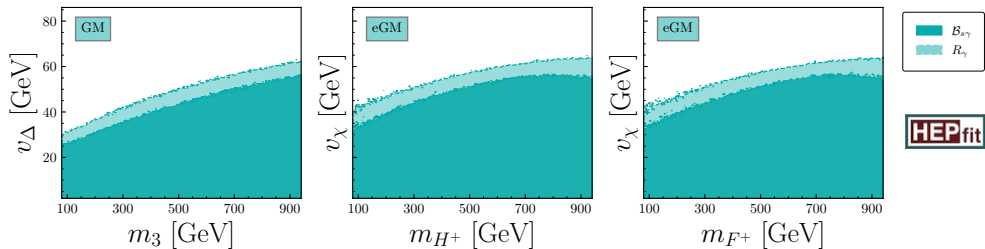


FIG. 2. Left: Constraints on  $m_3$  vs.  $v_\Delta$  plane from  $R_\gamma$  and  $\mathcal{B}_{s\gamma}$  for the GM model. Middle (Right): Constraints on  $m_{H^+}$  vs.  $v_\chi$  ( $m_{F^+}$  vs.  $v_\chi$ ) plane from  $R_\gamma$  and  $\mathcal{B}_{s\gamma}$  for the eGM model. The dark cyan regions are allowed from  $\mathcal{B}_{s\gamma}$ , and the light cyan regions are allowed from  $R_\gamma$  constraints at a 95.4% probability.

<sup>7</sup> For this, we sample the parameter space over the range,  $v_\Delta \in [0, 86]$  for the GM model, and  $v_\chi \in [0, 86]$  for the eGM model, and the BSM scalar masses,  $m_i \in [0.08, 1]$  TeV for both models. The remaining priors for the GM and eGM models are specified in Table 2.

<sup>8</sup> In this paper, we limit our analysis to one-loop corrections to  $\Delta C_7$  and  $\Delta C_8$  in both models. Higher-order corrections beyond one-loop can be significant and may further constrain the parameter space, but a detailed treatment of these effects lies beyond the scope of this work.

In Figure 3, we present the constraints on  $v_\chi$  as a function of  $m_{H^+}$ ,  $m_{F^+}$ , and  $m_{F^{++}}$  in the eGM model, derived from the LHC direct search limits. This result is based on the prior range of the eGM model given in Table 2. Since we vary  $m_H$  in the range  $m_H \in [90, 100]$  GeV, direct search limits for  $H$  are not considered in our analysis. Direct search constraint on the  $m_A$  vs.  $v_\chi$  plane is displayed in Figure 4, along with theoretical and other experimental constraints. The light orange regions in Figure 3 represent the parameter space allowed by heavy scalar searches, while the dark orange areas are allowed by the combined constraints from both light and heavy scalar searches at a 95.4% probability. In the left and middle panels, the parameter space of  $m_{H^+}, m_{F^+} < 200$  GeV is constrained by top quark decays,  $t \rightarrow H^+ b$  and  $t \rightarrow F^+ b$ . For  $m_{H^+}, m_{F^+} > 200$  GeV, direct searches for all heavy BSM scalars constrain the triplet VEV,  $v_\chi$ . When  $m_{H^+}, m_{F^+} > 700$  GeV, the decay modes  $H^+, F^+ \rightarrow W^+ A$  provide the most stringent constraints on  $v_\chi$ , shown in olive dashed lines in Figure 3. This is because the pseudoscalar masses,  $m_A > 600$  GeV is nearly excluded with a 95.4% probability from direct search limits, as shown in Figure 4.<sup>9</sup> In the right panel, the strongest constraint on the  $m_{F^{++}}$  vs.  $v_\chi$  plane for  $m_{F^{++}} > 200$  GeV comes from the direct search limits of  $F^{++}$ , shown in magenta dashed lines in Figure 3.<sup>10</sup> In contrast, the region with  $m_{F^{++}} < 200$  GeV remains unconstrained by direct searches for  $F^{++}$  alone. However, this low-mass region becomes constrained when the searches for light pseudoscalar  $A$  and light singly-charged scalars  $F^+$  and  $H^+$  are taken into account.

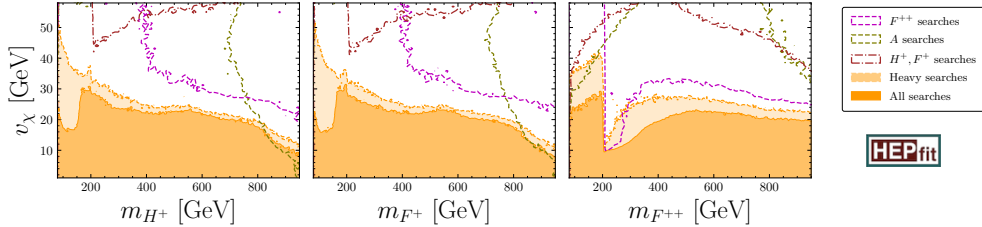


FIG. 3. Impacts of different direct search limits on  $v_\chi$  vs.  $m_{H^+}$ ,  $m_{F^+}$ , and  $m_{F^{++}}$  planes at a 95.4% probability. The regions above the magenta dashed, olive green dashed, and maroon dot-dashed lines are excluded from  $F^{++}$ ,  $A$ ,  $H^+$  (and  $F^+$ ) searches, respectively. The light orange regions are allowed by heavy scalar searches, and the dark orange areas indicate regions allowed from the combined fit to both light and heavy scalars direct search data. The direct search limits on the singly and doubly-charged scalars considered in this analysis are listed in Table 4.

Figure 4 presents the allowed range of  $v_\chi$  as a function of the pseudoscalar mass  $m_A$  in the eGM model.<sup>11</sup> The left panel displays the higher  $m_A$  mass range, while the right panel focuses on the lower mass region,  $m_A \in [10, 180]$  GeV. In the CP-conserving eGM model, the masses and mixing angles of singly-charged scalars  $H^+$  and  $F^+$ , together with the triplet VEV  $v_\chi$ , determine the pseudoscalar mass  $m_A$  [110]. As a result, the entire  $m_A - v_\chi$  parameter space is not accessible. The grey regions in Figure 4 denote the portion of the  $m_A$  vs.  $v_\chi$  plane allowed in the eGM model for a light Higgs  $H$  with  $m_H \in [90, 100]$  GeV without imposing any constraints. There exists an upper bound on  $m_A$  for any fixed value of  $v_\chi$ , and a lower bound on  $v_\chi$  for fixed  $m_A$  in the range  $m_A \in [10, 80]$  GeV, both arising solely from the model properties and parameter sampling. When theoretical constraints such as NLO unitarity and BFB conditions are imposed, these bounds become more stringent, causing the grey regions to shrink further into the green regions. The orange regions represent the parameter space consistent with direct search limits on

<sup>9</sup> Note that, the pseudoscalar mass  $m_A$  is not an independent parameter in the eGM model (see Eq. (10) of Ref. [110]).

<sup>10</sup> The region where  $m_{F^{++}} \sim 450$  GeV is less constrained due to a recent excess observed by ATLAS near 450 GeV [155] in the same-sign  $WW$  channel.

<sup>11</sup> In the GM model, the pseudoscalar and one of the singly-charged scalar masses are degenerate, so the lower bound on the pseudoscalar mass is determined by the LEP constraint on the charged scalar, which is around 80 GeV. In this work, we investigate how light the pseudoscalar  $A$  can be within the framework of the CP-conserving eGM model.

all BSM scalars in the eGM model. In the low-mass region, the direct search limit imposes a strong upper bound on  $v_\chi$ , effectively excluding the parameter space below approximately 80 GeV. In the range  $m_A \in [80, 180]$  GeV, direct search limits impose an upper bound on  $v_\chi$  of around 22 GeV, while for  $m_A > 180$  GeV, the upper bound increases to  $\sim 30$  GeV. The blue regions indicate the parameter space compatible with a combined fit to the 95 GeV Higgs signal strength data, along with all other experimental and theoretical constraints. Here, the 95 GeV signal strength data includes the  $\gamma\gamma$  and  $b\bar{b}$  decay channels, given in Table 1.<sup>12</sup> This combined fit further tightens the bounds on the triplet VEV, reducing the upper limit on  $v_\chi$  to about 12 GeV for  $m_A \in [80, 180]$  GeV, and to approximately 25 GeV for  $m_A > 180$  GeV.

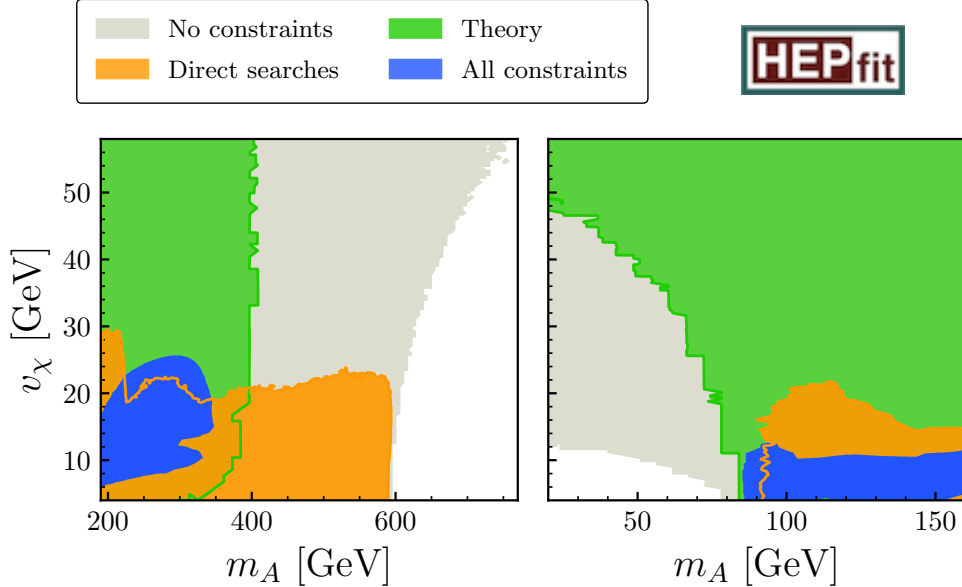


FIG. 4. Allowed region in the  $m_A$  vs.  $v_\chi$  plane for the eGM model. The grey regions denote the allowed region in the presence of a light Higgs  $H$  with  $m_H \in [90, 100]$  GeV without imposing any constraints. The green regions show the parameter space allowed by the theoretical constraints. The orange regions represent the parameter space consistent with direct search constraints on all BSM scalars in the eGM model. The blue region represents the parameter space allowed by a combined fit to the 95 GeV Higgs signal strengths in the  $\gamma\gamma$  and  $b\bar{b}$  channels, along with all the experimental and theoretical constraints.

In Figure 5, we present the allowed ranges for the BSM scalar masses and their mass differences in the eGM model, after applying both theoretical and experimental constraints. The green regions correspond to parameter space allowed solely by the theoretical bounds. For a comprehensive analysis of how theoretical constraints influence the parameter space, we refer the reader to Ref. [110]. The presence of a light BSM scalar  $H$  with  $m_H \in [90, 100]$  GeV introduces upper bounds on the other BSM scalar masses and mass differences, as reflected in the green region of Figure 5. In addition, imposing the combined Higgs signal strength data further restricts the triplet vacuum expectation value  $v_\chi$  and the mixing angle  $\alpha$  [110], reducing the allowed region to the red area.<sup>13</sup> Lastly, the blue region from the combined fit of all theoretical and experimental constraints, reveals a mass hierarchy among the heavy scalars. The hierarchy is determined by direct search constraints. As previously mentioned, we assume  $m_{F+} > m_{H+}$  with the possibility of eigenstate

<sup>12</sup> The  $H \rightarrow \tau\tau$  excess observed by CMS [34] (where  $H$  is a CP-even BSM scalar) is not consistent with the SM-like  $h$  signal strength data, and therefore is not considered in our analysis. For details, see Appendix B.

<sup>13</sup> In this work, combined Higgs signal strength data includes both the 125 GeV and 95 GeV Higgs signal strength data from LHC and LEP collider.



interchange depending on the parameter space. In panel II, when  $m_A$  is low, both the positive and negative regions of  $m_{F^0} - m_{F^+}$  are constrained from the direct search limits. When  $m_A$  is high, the eigenstate  $F^+$  corresponds to  $H^+$ , and the condition  $m_A = m_{H^+}$  must be satisfied within the parameter space.<sup>14</sup> As a result, the region around the diagonal line remains unconstrained. A similar feature is observed in panel I. For low  $m_A$ , both the positive and negative regions of  $m_{F^0} - m_{H^+}$  are constrained from the direct search limits. When  $m_A$  is high, the eigenstate  $H^+$  becomes  $F^+$ , and the corresponding region around  $m_{F^0} - m_{H^+} = 0$  remain unconstrained. Similarly, in panel III, the region around  $m_{F^0} - m_{F^{++}} = 0$  is also unconstrained. The same behavior is observed across the other panels in Figure 5, reflecting the interplay between singly-charged scalar eigenstate identification and mass degeneracy conditions in the eGM model under direct search constraints. All the mass planes in the eGM model are displayed in Figure 9 in Appendix C. From the combined fit, the regions where  $m_{F^{++}} > 600$  GeV,  $m_{F^+} > 350$  GeV,  $m_{F^0} > 580$  GeV,  $m_{H^+} > 590$  GeV,  $m_A > 350$  GeV, and their absolute mass differences above 250 GeV are excluded, at a 95.4% probability.

In Figure 6, we present the constraints on the triplet VEV  $v_\Delta$  as a function of BSM scalar masses within the GM model. The figure incorporates theoretical constraints, direct search limits,  $B$ -physics observables, and a combined fit to the 95 GeV Higgs signal strength data, along with all other relevant experimental and theoretical constraints.<sup>15</sup> The colour scheme follows that of Figures 2 and 4. As discussed in Section V, stringent LEP bounds on low-mass charged scalar necessitate a lower limit of 80 GeV on both  $m_3$  and  $m_5$  in our analysis. Theoretical constraints place an upper bound on these masses for a fixed  $v_\Delta$ , while  $B$ -physics data limit  $v_\Delta$  for a fixed  $m_3$ , as illustrated in Figure 2. In the left panel, the low  $m_3$  region is constrained by bounds from  $t \rightarrow H_3^+ b$  decays, while the region with  $m_3 > 180$  GeV is dominantly constrained by searches for the pseudoscalar  $H_3^0$  and the singly-charged scalar  $H_3^+$ . In the right panel, the region where  $m_5 < 200$  GeV remains unconstrained by direct searches, whereas for  $m_5 > 200$  GeV, the parameter space is significantly restricted by all heavy scalar searches. In the combined fit, the mass difference between  $m_5$  and  $m_3$  is tightly constrained (see Figure 7). As a result, in the low  $m_5$  region, the triplet VEV is indirectly constrained by limits on the VEV in the low  $m_3$  region. Similarly, in the high  $m_3$  region, the upper bound on the VEV is significantly reduced due to stringent constraints in the high  $m_5$  region from direct searches. The combined fit to all the experimental and theoretical constraints places an upper bound on  $v_\Delta$  of approximately 4 GeV for  $m_3 \in [80, 150]$  GeV and  $m_5 \in [80, 230]$  GeV. For higher masses, specifically  $m_3 \in [150, 320]$  GeV and  $m_5 \in [230, 530]$  GeV, the upper bound on  $v_\Delta$  relaxes to around 15 GeV.

Finally, in Figure 7, we present the allowed parameter space for the BSM scalar masses and their mass differences within the GM model. The colour scheme is consistent with that used in Figure 5. For a comprehensive discussion of the impact of theoretical constraints on the GM model's parameter space, we refer the reader to Ref. [110]. Fixing  $m_1 \in [90, 100]$  GeV imposes upper bounds on the masses and mass differences of the other BSM scalars, as shown in the green region of Figure 7. Theoretical constraints allow the mass difference  $m_5 - m_3$  to be either positive or negative. However, the combined Higgs signal strength data further restrict the triplet VEV  $v_\Delta$  and the mixing angle  $\alpha$  [110], thereby reducing allowed parameter space to the red region, and leads to a preferred mass hierarchy between  $m_3$  and  $m_5$ . This is because, in the GM model, the two trilinear parameters  $\mu_1$  and  $\mu_2$  are not constrained by theory bounds. Fixing  $m_1 \in [90, 100]$  GeV uniquely determines one of these parameters, while the other one is constrained by the Higgs signal strength data. As a result, the combined fit, including both theoretical constraints and

<sup>14</sup> Because  $m_A = m_{H^+}$  and  $m_{F^0} = m_{F^+} = m_{F^{++}}$  with the mixing angle  $\delta = 0$  represents a limiting case of the eGM model [110].

<sup>15</sup> We sample the parameter space over the BSM scalar masses,  $m_1, m_3, m_5 \in [0.08, 1]$  TeV when presenting the allowed parameter space from  $B$ -physics and direct search limits. The remaining priors for the GM model are given in Table 2.



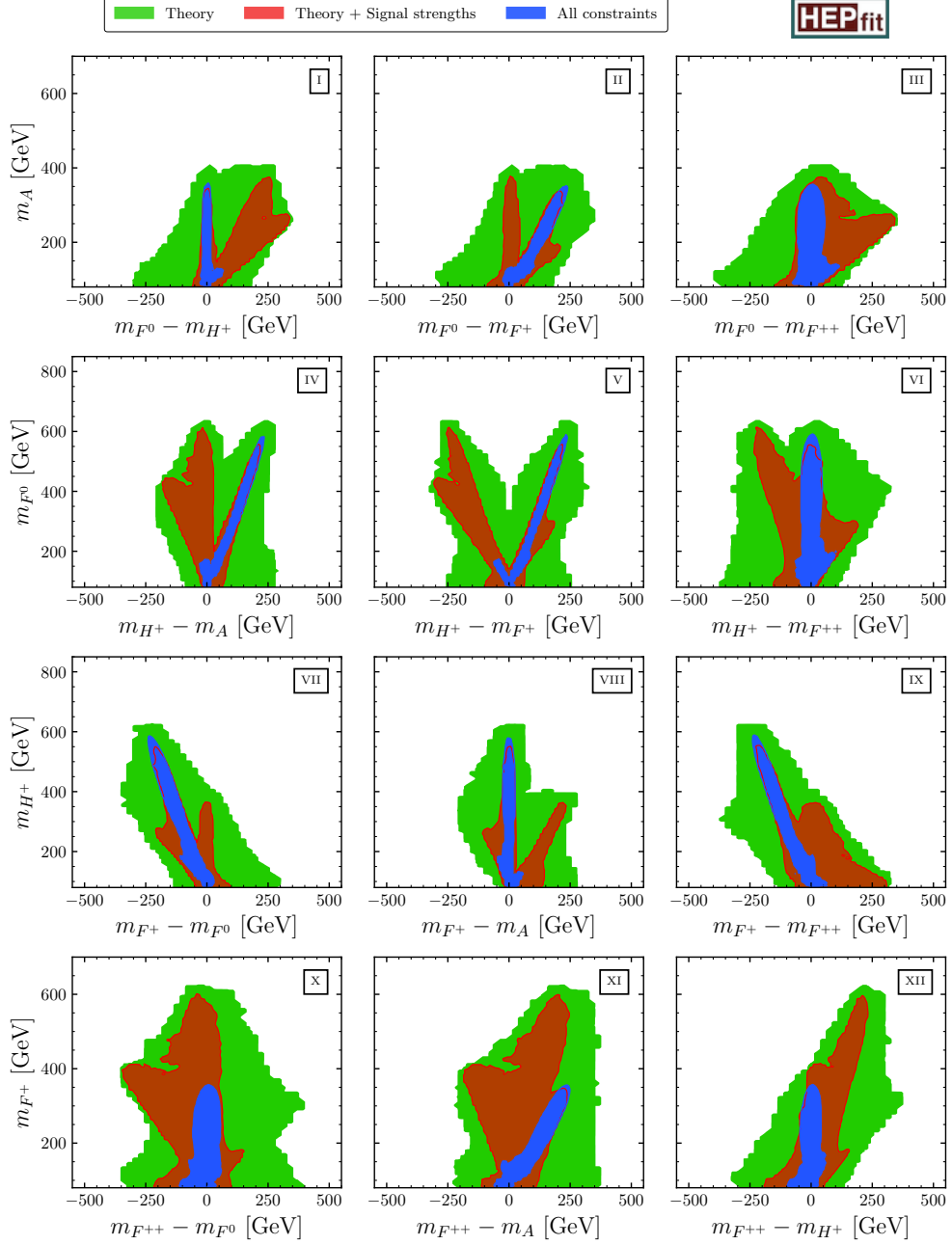


FIG. 5. Allowed regions in the  $m_i$  vs.  $(m_j - m_k)$  planes in the eGM model. The red regions show the parameter space allowed from a fit to the combined Higgs signal strength data, including theory bounds. The green and blue regions have the same meaning as in Figure 4.

signal strength data, leads to the mass hierarchy  $m_5 > m_3$  in the high mass region. The blue areas in Figure 7 are allowed from the combined fit to all the theoretical and experimental constraints. From the combined fit, the regions where  $m_5 > 530$  GeV,  $m_3 > 320$  GeV, and their mass difference is above 210 GeV, are excluded at a 95.4% probability.

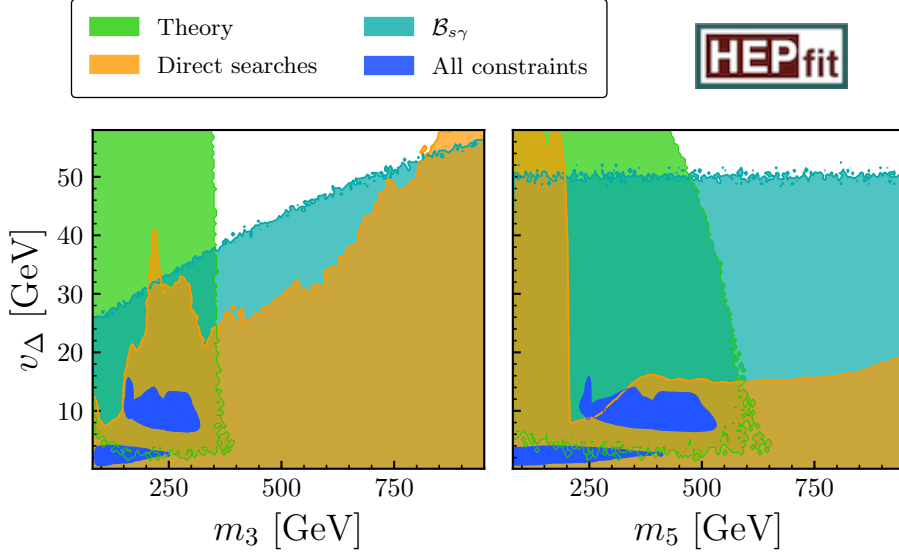


FIG. 6. Allowed region in the  $m_3$  vs.  $v_\Delta$  plane (left) and  $m_5$  vs.  $v_\Delta$  plane (right) for the GM model. The green, cyan, orange, and blue regions have the same meaning as in Figures 2 and 4.

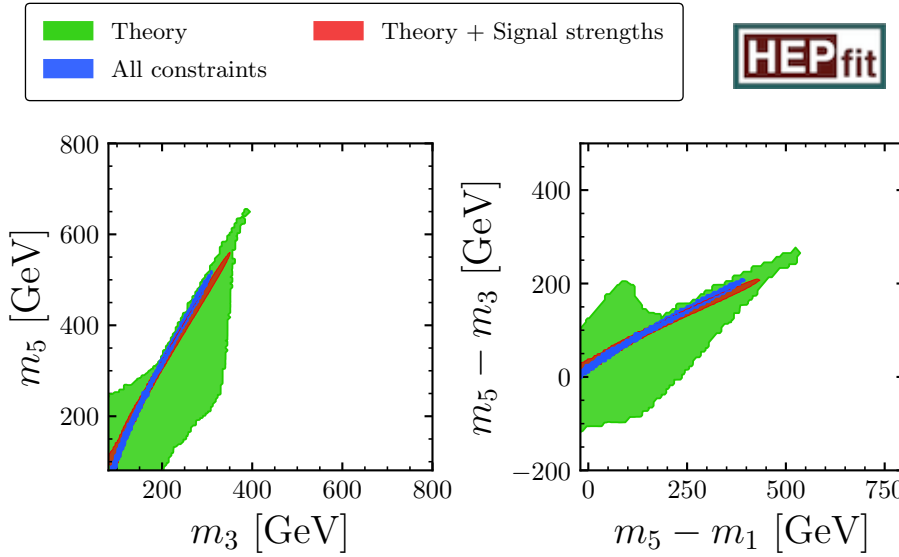


FIG. 7. Allowed regions in the mass (left) and mass difference (right) planes in the GM model. The green, red, and blue regions have the same meaning as in Figure 5.

## VII. CONCLUSIONS

We have presented the results of the global fits to the most recent data for both the GM and eGM models incorporating a light CP-even BSM scalar with a mass in the range  $[90, 100]$  GeV. Our global fits rely on Bayesian statistics and are performed using the open-source code **HEPfit**.

We compute the New Physics (NP) contributions to the Wilson coefficients,  $\Delta C_7$  and  $\Delta C_8$ , within the eGM model at one-loop level, and performed a phenomenological study using the updated SM predictions of the  $B$ -physics observables  $\mathcal{B}_{s\gamma}$  and  $R_\gamma$  from [130]. Each of these observables puts

a constraint on the triplet VEV as a function of charged scalar masses. We show that the latest result from HFLAV on  $B_{s\gamma}$  imposes a dominant constraint on the parameter space, with weaker bounds in the eGM model compared to the GM model. In the GM model, latest limit on  $B_{s\gamma}$  from HFLAV slightly tighten the parameter space relative to the previous analysis [93].

We have performed fits to both heavy and light BSM scalar searches for the eGM model, varying the mass of the lightest custodial singlet  $H$  in the range  $m_H \in [90, 100]$  GeV. We categorise the searches by decay products and compare the exclusion strength of individual ATLAS and CMS analyses on the production cross-section times branching ratio as a function of mass. Combining all decay channels, we show their impact on the triplet VEV as a function of BSM scalar masses in the eGM model. We observe that although  $B$ -physics observables constrain the triplet VEV in the low-mass region, the most stringent limits in this region come from LHC direct searches. For singly- and doubly-charged scalar masses below 200 GeV, the combined effect of light pseudoscalar and singly-charged scalar searches places strong constraints on the triplet VEV of the eGM model. Combined fit to the direct searches with theoretical constraints disfavour the region where  $m_A \lesssim 80$  GeV, at a 95.4% probability. For  $m_A \in [80, 180]$  GeV, direct searches impose an upper bound on  $v_\chi$  of around 22 GeV, which relaxes to  $\sim 30$  GeV for  $m_A > 180$  GeV.

As a case study, we consider the diphoton and ditau excesses observed at the LHC, along with the  $b\bar{b}$  excess reported by LEP at a mass around 95 GeV. We show that the lighter (CP-even) custodial singlet  $H$  can explain the observed 95 GeV excesses in both the CP-conserving GM and eGM models without violating NLO unitarity and BFB conditions. Global fits of both models show that the  $H \rightarrow \gamma\gamma$  and  $b\bar{b}$  data from the LHC and LEP, respectively, are fully compatible with the measured SM-like  $h$  signal strength data, whereas the  $H \rightarrow \tau^+\tau^-$  data reported by CMS collaborations is inconsistent with SM-like  $h$  signal strength data. From the combined signal strength data, we find  $|\kappa_V^H| < 0.4$  and  $|\kappa_F^H| < 0.15$  in both models, at a 95.4% probability.

For the GM model, we update the direct search constraints by including the latest data on heavy scalar searches from LHC and, for the first time, incorporate light scalar searches into the global fits. The region  $m_3 < 160$  GeV is constrained by top quark decays ( $t \rightarrow H_3^+ b$ ) with the triplet VEV above 12 GeV is disfavour at a 95.4% probability, while  $m_5 < 200$  GeV remains unconstrained by direct searches.

Incorporating our recently calculated NLO unitarity and BFB conditions [110], we performed an updated global analysis of both the GM and eGM models, including the most recent experimental data. Fixing  $m_1$  or  $m_H = 95.4$  GeV, we find the following ranges of the model parameters, with a 95.4% probability, while marginalising over all other parameters: In the eGM model, the triplet VEV cannot exceed 12 GeV for BSM scalar masses below 160 GeV and approximately 25 GeV for BSM scalar masses above 160 GeV. The masses of additional BSM scalars:  $m_{F^{++}} < 600$  GeV,  $m_{F^+} < 350$  GeV,  $m_{F^0} < 580$  GeV,  $m_{H^+} < 590$  GeV, and  $m_A < 350$  GeV. The maximum mass splitting is of around 120 GeV within the members of each custodial multiplet, and up to 250 GeV between the members of different multiplets. In the GM model, these constraints become more stringent: the triplet VEV is limited to below 15 GeV if the additional BSM scalar masses are above 160 GeV, which tightens to 4 GeV once the BSM scalar masses are below 160 GeV. The masses of the quintet  $m_5$  and the triplet  $m_3$  are restricted to be below 530 GeV and 320 GeV, respectively. A mass hierarchy,  $m_5 > m_3$ , is favoured in the high-mass region, with the mass splitting constrained to be less than 210 GeV.

In summary, although the current constraints on the triplet vacuum expectation value in the low-mass regime of the GM model are stringent, our results show that sizeable regions of the eGM model's parameter space remain viable and unexplored. These findings motivate dedicated experimental searches for light neutral and charged scalars. We present the upper limit of the

other BSM scalar masses in both models in the presence of a 95 GeV BSM scalar. Hence, our results address a key question: whether the GM or eGM model can simultaneously accommodate the observed 95 GeV excess and other excesses reported at the LHC.

## ACKNOWLEDGMENTS

We thank Debtosh Chowdhury and Anirban Kundu for useful discussions and their valuable comments on the manuscript. S.S. acknowledges funding from the MHRD, Government of India, under the Prime Minister's Research Fellows (PMRF) Scheme. The work of P.M. is supported by the funding from the ANRF, Government of India, under grant CRG/2021/007579.

## Appendix A

In this appendix, we provide the latest direct searches of the charged scalars. In Table 4, we list all the productions and decay channels of the charged scalars relevant to the eGM models.

Channel	Experiment	Mass range [TeV]	$\mathcal{L}$ [fb <sup>-1</sup> ]
$pp \rightarrow H^\pm, F^\pm \rightarrow \tau^\pm \nu$	ATLAS [156]	[0.18;1]	19.5
	CMS [157]	[0.18;0.6]	19.7
$pp \rightarrow H^\pm, F^\pm \rightarrow \tau^\pm \nu$	ATLAS [158]	[0.2;2]	36.1
	CMS [159]	[0.08;3]	35.9
$pp \rightarrow H^\pm, F^\pm \rightarrow \tau^\pm \nu$	ATLAS [156]	[0.18;1]	19.5
	CMS [157]	[0.18;0.6]	19.7
$pp \rightarrow H^\pm, F^\pm \rightarrow \tau^\pm \nu$	ATLAS [158]	[0.2;2]	36.1
	CMS [159]	[0.08;3]	35.9
$pp \rightarrow H^\pm, F^\pm \rightarrow tb$	CMS [160]	[0.2;3]	35.9
	ATLAS [161]	[0.2;2]	139
$pp \rightarrow H^+, F^+ \rightarrow t\bar{b}$	CMS [157]	[0.18;0.6]	19.7
	ATLAS [162]	[0.2;0.6]	20.3
$WZ \rightarrow H^+, F^+ \rightarrow WZ [\rightarrow (qq)(\ell\ell)]$	ATLAS [163]	[0.2;1]	20.3
$WZ \rightarrow H^+, F^+ \rightarrow WZ [\rightarrow (\ell\nu)(\ell\ell)]$	CMS [24]	[0.2;3]	137
	ATLAS [155]	[0.2;3]	140
$VV \rightarrow F^{++} \rightarrow WW [\rightarrow (\ell\nu)(\ell\nu)]$	CMS [164]	[0.2;0.8]	19.4
$VV \rightarrow F^{++} \rightarrow WW [\rightarrow (\ell\nu)(\ell\nu)]$	CMS [24]	[0.2;3]	137
	ATLAS [155]	[0.2;3]	140
$pp \rightarrow F^{\pm\pm} F^{\pm\pm} \rightarrow W^\pm W^\pm W^\pm W^\pm$	ATLAS [165]	[0.2;0.6]	139

TABLE 4. List of direct searches in LHC for singly- and doubly-charged scalars in the eGM model. Parentheses denote the final state decays of SM particles produced from the decays of BSM particles.

## Appendix B

Here, we have considered the observed hints of a light Higgs boson near 95 GeV from both the LHC [30, 31] and LEP [32], and investigate whether a CP-even scalar,  $H$ , with a mass of 95.4 GeV can account for these hints, within the frameworks of the CP-conserving GM and eGM models. The grey regions in Figure 8 illustrate the prior range in the  $\kappa_f^H - \kappa_V^H$  plane for a light Higgs boson  $H$ , where  $m_H < m_h \approx 125$  GeV.<sup>16</sup> The yellow regions correspond to the parameter space allowed by the combined signal strength measurements of the SM-like Higgs boson  $h$  decaying into all final states, as summarised in Table 2 of [141] and in Tables 4 and 5 of [110]. The light blue regions show the parameter space compatible with the observed 95 GeV Higgs signal strength in the  $\tau^+\tau^-$  decay channel, based on the value listed in Table 1. The blue regions indicate the parameter space allowed by a combined fit to the 95 GeV Higgs signal strengths in the  $\gamma\gamma$  and  $b\bar{b}$  channels, given in Table 1, incorporating all other experimental and theoretical constraints. Notably, the blue region lies entirely within the yellow region, indicating that the  $H \rightarrow \gamma\gamma, b\bar{b}$  excesses observed by the LHC and LEP are compatible with the measured SM-like  $h$  signal strengths in both the GM and eGM models. In contrast, the CMS observed  $H \rightarrow \tau^+\tau^-$  excess [34] is not consistent with the SM-like  $h$  signal strength data, shown in the light blue region. It was recently shown in Ref. [55] that explaining the CMS ditau excess with a CP-even resonance is in tension with the absence of a corresponding excess in CMS searches for  $t\bar{t}$ -associated production of a scalar decaying into tau pairs, based on the full Run 2 dataset at 13 TeV [166]. Therefore, we exclude the  $H \rightarrow \tau^+\tau^-$  signal strength data in the combined fit of both the models.

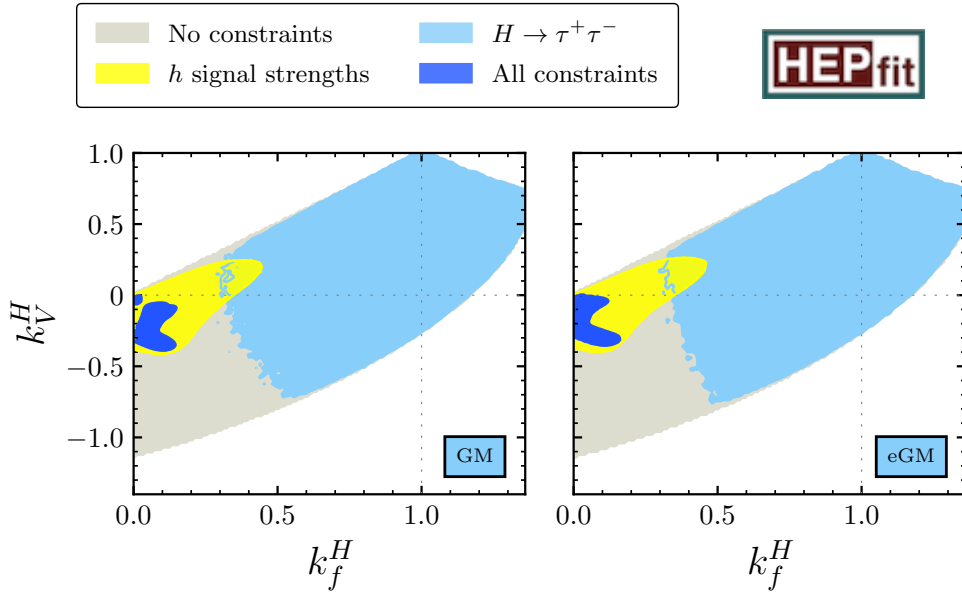


FIG. 8. Left:  $\kappa_f^H$  vs.  $\kappa_V^H$  plane for the GM model. Right:  $\kappa_f^H$  vs.  $\kappa_V^H$  plane for the eGM model. The grey regions are the allowed parameter space for a light Higgs  $H$  without imposing any constraints, where  $m_H < m_h \approx 125$  GeV. The yellow regions indicate the allowed parameter space consistent with the SM-like Higgs boson  $h$  signal strengths. The light blue regions correspond to the parameter space compatible with the observed  $H$  signal strength in the  $\tau\tau$  decay channel, where  $m_H = 95.4$  GeV. The blue region represents the parameter space allowed by a combined fit to the  $H$  signal strengths in the  $\gamma\gamma$  and  $b\bar{b}$  channels, along with all other experimental and theoretical constraints.

<sup>16</sup> In contrast to the case with  $m_H > m_h$ , where the mixing angle  $\alpha < 0$  is generally favoured (see Refs. [96, 110]), our analysis focuses on the scenario where  $m_H < m_h$ , for which positive values of  $\alpha$  are typically preferred. We therefore sample in the region  $\alpha \in [0, \pi/2]$ .

## Appendix C

In this appendix, we provide the supplementary figures for the eGM model. The allowed regions in the mass planes are shown in Figure 9. The colors in Figure 9 have the same meaning as in Figure 5. In panels II and VII, we see that the combined fit reveals a mass hierarchy  $m_{F^0} > m_A$  and  $m_{F^{++}} > m_A$  in the high-mass region. In contrast, there is no preferred mass hierarchy among the members of each custodial multiplets.

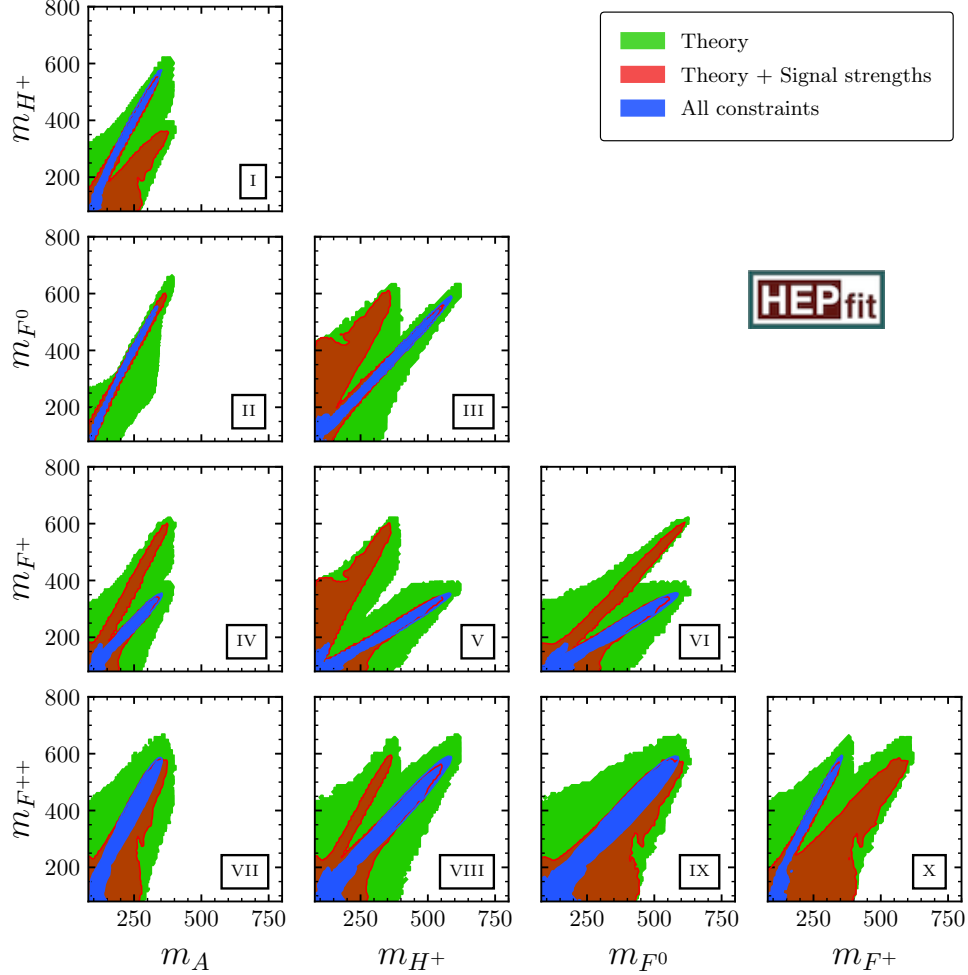


FIG. 9. Allowed regions in the mass planes in the eGM model. The green, red, and blue regions have the same meaning as in Figure 5.

- 
- [1] ATLAS collaboration, *Observation of a new particle in the search for the Standard Model Higgs boson with the ATLAS detector at the LHC*, *Phys. Lett. B* **716** (2012) 1 [[1207.7214](#)].
  - [2] CMS collaboration, *Observation of a New Boson at a Mass of 125 GeV with the CMS Experiment at the LHC*, *Phys. Lett. B* **716** (2012) 30 [[1207.7235](#)].
  - [3] ATLAS, CMS collaboration, *Measurements of the Higgs boson production and decay rates and constraints on its couplings from a combined ATLAS and CMS analysis of the LHC pp collision data at  $\sqrt{s} = 7$  and 8 TeV*, *JHEP* **08** (2016) 045 [[1606.02266](#)].

- [4] ATLAS collaboration, *Higgs boson production cross-section measurements and their EFT interpretation in the  $4\ell$  decay channel at  $\sqrt{s}=13$  TeV with the ATLAS detector*, *Eur. Phys. J. C* **80** (2020) 957 [2004.03447].
- [5] ATLAS collaboration, *A search for the  $Z\gamma$  decay mode of the Higgs boson in  $pp$  collisions at  $\sqrt{s} = 13$  TeV with the ATLAS detector*, *Phys. Lett. B* **809** (2020) 135754 [2005.05382].
- [6] ATLAS collaboration, *Measurements of  $WH$  and  $ZH$  production in the  $H \rightarrow b\bar{b}$  decay channel in  $pp$  collisions at 13 TeV with the ATLAS detector*, *Eur. Phys. J. C* **81** (2021) 178 [2007.02873].
- [7] ATLAS collaboration, *A search for the dimuon decay of the Standard Model Higgs boson with the ATLAS detector*, *Phys. Lett. B* **812** (2021) 135980 [2007.07830].
- [8] CMS collaboration, *Evidence for Higgs boson decay to a pair of muons*, *JHEP* **01** (2021) 148 [2009.04363].
- [9] ATLAS collaboration, *Measurements of Higgs bosons decaying to bottom quarks from vector boson fusion production with the ATLAS experiment at  $\sqrt{s} = 13$  TeV*, *Eur. Phys. J. C* **81** (2021) 537 [2011.08280].
- [10] CMS collaboration, *Measurements of production cross sections of the Higgs boson in the four-lepton final state in proton–proton collisions at  $\sqrt{s} = 13$  TeV*, *Eur. Phys. J. C* **81** (2021) 488 [2103.04956].
- [11] CMS collaboration, *Measurements of Higgs boson production cross sections and couplings in the diphoton decay channel at  $\sqrt{s} = 13$  TeV*, *JHEP* **07** (2021) 027 [2103.06956].
- [12] ATLAS collaboration, *Measurement of Higgs boson decay into  $b$ -quarks in associated production with a top-quark pair in  $pp$  collisions at  $\sqrt{s} = 13$  TeV with the ATLAS detector*, *JHEP* **06** (2022) 097 [2111.06712].
- [13] ATLAS collaboration, *Measurements of Higgs boson production cross-sections in the  $H \rightarrow \tau^+\tau^-$  decay channel in  $pp$  collisions at  $\sqrt{s} = 13$  TeV with the ATLAS detector*, *JHEP* **08** (2022) 175 [2201.08269].
- [14] CMS collaboration, *Search for Higgs boson decays to a  $Z$  boson and a photon in proton-proton collisions at  $\sqrt{s} = 13$  TeV*, *JHEP* **05** (2023) 233 [2204.12945].
- [15] CMS collaboration, *Measurements of Higgs boson production in the decay channel with a pair of  $\tau$  leptons in proton–proton collisions at  $\sqrt{s} = 13$  TeV*, *Eur. Phys. J. C* **83** (2023) 562 [2204.12957].
- [16] CMS collaboration, *Measurements of the Higgs boson production cross section and couplings in the  $W$  boson pair decay channel in proton-proton collisions at  $\sqrt{s} = 13$  TeV*, *Eur. Phys. J. C* **83** (2023) 667 [2206.09466].
- [17] CMS collaboration, *A portrait of the Higgs boson by the CMS experiment ten years after the discovery.*, *Nature* **607** (2022) 60 [2207.00043].
- [18] ATLAS collaboration, *A detailed map of Higgs boson interactions by the ATLAS experiment ten years after the discovery*, *Nature* **607** (2022) 52 [2207.00092].
- [19] ATLAS collaboration.
- [20] ATLAS collaboration, *Measurement of the properties of Higgs boson production at  $\sqrt{s} = 13$  TeV in the  $H \rightarrow \gamma\gamma$  channel using  $139 \text{ fb}^{-1}$  of  $pp$  collision data with the ATLAS experiment*, *JHEP* **07** (2023) 088 [2207.00348].
- [21] CMS collaboration, *Measurement of the Higgs boson production via vector boson fusion and its decay into bottom quarks in proton-proton collisions at  $\sqrt{s} = 13$  TeV*, *JHEP* **01** (2024) 173 [2308.01253].
- [22] CMS collaboration, *Search for a doubly-charged Higgs boson with  $\sqrt{s} = 8$  TeV  $pp$  collisions at the CMS experiment*, .
- [23] ATLAS collaboration, *Measurement and interpretation of same-sign  $W$  boson pair production in association with two jets in  $pp$  collisions at  $\sqrt{s} = 13$  TeV with the ATLAS detector*, .
- [24] CMS collaboration, *Search for charged Higgs bosons produced in vector boson fusion processes and decaying into vector boson pairs in proton–proton collisions at  $\sqrt{s} = 13$  TeV*, *Eur. Phys. J. C* **81** (2021) 723 [2104.04762].
- [25] ATLAS collaboration, *Search for resonant  $WZ$  production in the fully leptonic final state in proton–proton collisions at  $\sqrt{s} = 13$  TeV with the ATLAS detector*, *Eur. Phys. J. C* **83** (2023) 633 [2207.03925].
- [26] CMS collaboration, *Search for heavy Higgs bosons decaying to a top quark pair in proton-proton collisions at  $\sqrt{s} = 13$  TeV*, *JHEP* **04** (2020) 171 [1908.01115].
- [27] ATLAS collaboration, *Search for Higgs boson pair production in association with a vector boson in  $pp$  collisions at  $\sqrt{s} = 13$  TeV with the ATLAS detector*, .



- [28] CMS collaboration, *Search for new resonances in the diphoton final state in the mass range between 80 and 115 GeV in pp collisions at  $\sqrt{s} = 8$  TeV*, .
- [29] CMS collaboration, *Search for a standard model-like Higgs boson in the mass range between 70 and 110 GeV in the diphoton final state in proton-proton collisions at  $\sqrt{s} = 8$  and 13 TeV*, *Phys. Lett. B* **793** (2019) 320 [[1811.08459](#)].
- [30] CMS collaboration, *Search for a standard model-like Higgs boson in the mass range between 70 and 110 GeV in the diphoton final state in proton-proton collisions at  $\sqrt{s} = 13$  TeV*, [2405.18149](#).
- [31] ATLAS collaboration, *Search for diphoton resonances in the 66 to 110 GeV mass range using pp collisions at  $\sqrt{s} = 13$  TeV with the ATLAS detector*, [2407.07546](#).
- [32] LEP WORKING GROUP FOR HIGGS BOSON SEARCHES, ALEPH, DELPHI, L3, OPAL collaboration, *Search for the standard model Higgs boson at LEP*, *Phys. Lett. B* **565** (2003) 61 [[hep-ex/0306033](#)].
- [33] ALEPH, DELPHI, L3, OPAL, LEP WORKING GROUP FOR HIGGS BOSON SEARCHES collaboration, *Search for neutral MSSM Higgs bosons at LEP*, *Eur. Phys. J. C* **47** (2006) 547 [[hep-ex/0602042](#)].
- [34] CMS collaboration, *Searches for additional Higgs bosons and for vector leptoquarks in  $\tau\tau$  final states in proton-proton collisions at  $\sqrt{s} = 13$  TeV*, *JHEP* **07** (2023) 073 [[2208.02717](#)].
- [35] G. Cacciapaglia, A. Deandrea, S. Gascon-Shotkin, S. Le Corre, M. Lethuillier and J. Tao, *Search for a lighter Higgs boson in Two Higgs Doublet Models*, *JHEP* **12** (2016) 068 [[1607.08653](#)].
- [36] J. Cao, X. Guo, Y. He, P. Wu and Y. Zhang, *Diphoton signal of the light Higgs boson in natural NMSSM*, *Phys. Rev. D* **95** (2017) 116001 [[1612.08522](#)].
- [37] P.J. Fox and N. Weiner, *Light Signals from a Lighter Higgs*, *JHEP* **08** (2018) 025 [[1710.07649](#)].
- [38] D. Liu, J. Liu, C.E.M. Wagner and X.-P. Wang, *A Light Higgs at the LHC and the B-Anomalies*, *JHEP* **06** (2018) 150 [[1805.01476](#)].
- [39] F. Domingo, S. Heinemeyer, S. Paßehr and G. Weiglein, *Decays of the neutral Higgs bosons into SM fermions and gauge bosons in the CP-violating NMSSM*, *Eur. Phys. J. C* **78** (2018) 942 [[1807.06322](#)].
- [40] T. Biekötter, M. Chakraborti and S. Heinemeyer, *A 96 GeV Higgs boson in the N2HDM*, *Eur. Phys. J. C* **80** (2020) 2 [[1903.11661](#)].
- [41] J.M. Cline and T. Toma, *Pseudo-Goldstone dark matter confronts cosmic ray and collider anomalies*, *Phys. Rev. D* **100** (2019) 035023 [[1906.02175](#)].
- [42] A. Kundu, S. Maharana and P. Mondal, *A 96 GeV scalar tagged to dark matter models*, *Nucl. Phys. B* **955** (2020) 115057 [[1907.12808](#)].
- [43] J. Cao, X. Jia, Y. Yue, H. Zhou and P. Zhu, *96 GeV diphoton excess in seesaw extensions of the natural NMSSM*, *Phys. Rev. D* **101** (2020) 055008 [[1908.07206](#)].
- [44] A.A. Abdelalim, B. Das, S. Khalil and S. Moretti, *Di-photon decay of a light Higgs state in the BLSSM*, *Nucl. Phys. B* **985** (2022) 116013 [[2012.04952](#)].
- [45] T. Biekötter, A. Grohsjean, S. Heinemeyer, C. Schwanenberger and G. Weiglein, *Possible indications for new Higgs bosons in the reach of the LHC: N2HDM and NMSSM interpretations*, *Eur. Phys. J. C* **82** (2022) 178 [[2109.01128](#)].
- [46] A. Crivellin, Y. Fang, O. Fischer, S. Bhattacharya, M. Kumar, E. Malwa et al., *Accumulating evidence for the associated production of a new Higgs boson at the LHC*, *Phys. Rev. D* **108** (2023) 115031 [[2109.02650](#)].
- [47] S. Heinemeyer, C. Li, F. Lika, G. Moortgat-Pick and S. Paasch, *Phenomenology of a 96 GeV Higgs boson in the 2HDM with an additional singlet*, *Phys. Rev. D* **106** (2022) 075003 [[2112.11958](#)].
- [48] T. Biekötter, S. Heinemeyer and G. Weiglein, *Mounting evidence for a 95 GeV Higgs boson*, *JHEP* **08** (2022) 201 [[2203.13180](#)].
- [49] T. Biekötter, S. Heinemeyer and G. Weiglein, *Excesses in the low-mass Higgs-boson search and the W-boson mass measurement*, *Eur. Phys. J. C* **83** (2023) 450 [[2204.05975](#)].
- [50] R. Benbrik, M. Boukidi, S. Moretti and S. Semlali, *Explaining the 96 GeV Di-photon anomaly in a generic 2HDM Type-III*, *Phys. Lett. B* **832** (2022) 137245 [[2204.07470](#)].
- [51] S. Iguro, T. Kitahara, Y. Omura and H. Zhang, *Chasing the two-Higgs doublet model in the di-Higgs boson production*, *Phys. Rev. D* **107** (2023) 075017 [[2211.00011](#)].
- [52] S. Iguro, T. Kitahara and Y. Omura, *Scrutinizing the 95–100 GeV di-tau excess in the top associated process*, *Eur. Phys. J. C* **82** (2022) 1053 [[2205.03187](#)].

- [53] A. Kundu, A. Le Yaouanc, P. Mondal and F. Richard, *Searches for scalars at LHC and interpretation of the findings*, in *2022 ECFA Workshop on  $e+e-$  Higgs/EW/Top factories*, 11, 2022 [[2211.11723](#)].
- [54] W. Li, H. Qiao and J. Zhu, *Light Higgs boson in the NMSSM confronted with the CMS di-photon and di-tau excesses\**, *Chin. Phys. C* **47** (2023) 123102 [[2212.11739](#)].
- [55] T. Biekötter, S. Heinemeyer and G. Weiglein, *The CMS di-photon excess at 95 GeV in view of the LHC Run 2 results*, *Phys. Lett. B* **846** (2023) 138217 [[2303.12018](#)].
- [56] D. Azevedo, T. Biekötter and P.M. Ferreira, *2HDM interpretations of the CMS diphoton excess at 95 GeV*, *JHEP* **11** (2023) 017 [[2305.19716](#)].
- [57] T. Biekötter, S. Heinemeyer and G. Weiglein, *95.4 GeV diphoton excess at ATLAS and CMS*, *Phys. Rev. D* **109** (2024) 035005 [[2306.03889](#)].
- [58] A. Belyaev, R. Benbrik, M. Boukidi, M. Chakraborti, S. Moretti and S. Semmlali, *Explanation of the hints for a 95 GeV Higgs boson within a 2-Higgs Doublet Model*, *JHEP* **05** (2024) 209 [[2306.09029](#)].
- [59] S. Ashanujjaman, S. Banik, G. Coloretti, A. Crivellin, B. Mellado and A.-T. Mulaudzi,  *$SU(2)_L$  triplet scalar as the origin of the 95 GeV excess?*, *Phys. Rev. D* **108** (2023) L091704 [[2306.15722](#)].
- [60] J.A. Aguilar-Saavedra, H.B. Câmara, F.R. Joaquim and J.F. Seabra, *Confronting the 95 GeV excesses within the  $U(1)'$ -extended next-to-minimal 2HDM*, *Phys. Rev. D* **108** (2023) 075020 [[2307.03768](#)].
- [61] J. Dutta, J. Lahiri, C. Li, G. Moortgat-Pick, S.F. Tabira and J.A. Ziegler, *Dark matter phenomenology in 2HDMS in light of the 95 GeV excess*, *Eur. Phys. J. C* **84** (2024) 926 [[2308.05653](#)].
- [62] A. Ahriche, *95 GeV excess in the Georgi-Machacek model: Single or twin peak resonance*, *Phys. Rev. D* **110** (2024) 035010 [[2312.10484](#)].
- [63] T.-K. Chen, C.-W. Chiang, S. Heinemeyer and G. Weiglein, *95 GeV Higgs boson in the Georgi-Machacek model*, *Phys. Rev. D* **109** (2024) 075043 [[2312.13239](#)].
- [64] G. Arcadi, G. Busoni, D. Cabo-Almeida and N. Krishnan, *Is there a scalar or pseudoscalar at 95 GeV?*, *Phys. Rev. D* **110** (2024) 115028 [[2311.14486](#)].
- [65] P.S.B. Dev, R.N. Mohapatra and Y. Zhang, *Explanation of the 95 GeV  $\gamma\gamma$  and  $bb^-$  excesses in the minimal left-right symmetric model*, *Phys. Lett. B* **849** (2024) 138481 [[2312.17733](#)].
- [66] R. Benbrik, M. Boukidi and S. Moretti, *Superposition of CP-even and CP-odd Higgs resonances: Explaining the 95 GeV excesses within a two-Higgs-doublet model*, *Phys. Rev. D* **110** (2024) 115030 [[2405.02899](#)].
- [67] J. Lian, *95 GeV excesses in the  $Z3$ -symmetric next-to-minimal supersymmetric standard model*, *Phys. Rev. D* **110** (2024) 115018 [[2406.10969](#)].
- [68] J.-L. Yang, M.-H. Guo, W.-H. Zhang, H.-B. Zhang and T.-F. Feng, *Explaining the possible 95 GeV excesses in the  $B$ - $L$  symmetric SSM*, [2406.01926](#).
- [69] A. Khanna, S. Moretti and A. Sarkar, *Explaining 95 (or so) GeV Anomalies in the 2-Higgs Doublet Model Type-I*, [2409.02587](#).
- [70] B. Ait-Ouazghour, M. Chabab and K. Goure, *Unified Interpretation of 95 GeV Excesses in the Two Higgs Doublet type II Seesaw Model*, [2410.11140](#).
- [71] A. Arhrib, K.H. Phan, V.Q. Tran and T.-C. Yuan, *When Standard Model Higgs Meets Its Lighter 95 GeV Higgs*, [2405.03127](#).
- [72] S. Gao, S.-M. Zhao, S. Di, X.-X. Dong and T.-F. Feng, *A 95 GeV Higgs Boson in the  $U(1)_X$  model*, [2411.13261](#).
- [73] A. Kundu, P. Mondal and G. Moulataka, *Indications for new scalar resonances at the LHC and a possible interpretation*, [2411.14126](#).
- [74] T. Mondal, S. Moretti and P. Sanyal, *On the CP Nature of the ‘95 GeV’ Anomalies*, [2412.00474](#).
- [75] S. Banik, G. Coloretti, A. Crivellin and H.E. Haber, *Correlating  $A \rightarrow \gamma\gamma$  with electric dipole moments in the two Higgs doublet model in light of the diphoton excesses at 95 GeV and 152 GeV*, *Phys. Rev. D* **111** (2025) 075021 [[2412.00523](#)].
- [76] A. Hmissou, S. Moretti and L. Rahili, *Investigating the 95 GeV Higgs Boson Excesses within the  $I(1+2)$ HDM*, [2502.03631](#).
- [77] X. Du, H. Liu and Q. Chang, *Interpretation of 95 GeV Excess within the Georgi-Machacek Model in Light of Positive Definiteness Constraints*, [2502.06444](#).
- [78] Z. Li, N. Liu and B. Zhu, *Interplay of 95 GeV Diphoton Excess and Dark Matter in Supersymmetric Triplet Model*, [2504.21273](#).

- [79] H. Xu, Y. Wang, X.-F. Han and L. Wang, *95 GeV Higgs boson and nano-Hertz gravitational waves from domain walls in the N2HDM*, [2505.03592](#).
- [80] R. Benbrik, M. Boukidi, K. Kahime, S. Moretti, L. Rahili and B. Taki, *Exploring Potential Higgs Resonances at 650 GeV and 95 GeV in the 2HDM Type III*, [2505.07811](#).
- [81] H. Georgi and M. Machacek, *Doubly charged Higgs bosons*, *Nucl. Phys. B* **262** (1985) 463.
- [82] M.S. Chanowitz and M. Golden, *Higgs Boson Triplets With  $M(W) = M(Z) \cos \theta_W$* , *Phys. Lett. B* **165** (1985) 105.
- [83] J.F. Gunion, R. Vega and J. Wudka, *Higgs triplets in the standard model*, *Phys. Rev. D* **42** (1990) 1673.
- [84] J.F. Gunion, R. Vega and J. Wudka, *Naturalness problems for  $\rho = 1$  and other large one loop effects for a standard model Higgs sector containing triplet fields*, *Phys. Rev. D* **43** (1991) 2322.
- [85] M. Aoki, S. Kanemura and K. Yagyu, *Testing the Higgs triplet model with the mass difference at the LHC*, *Phys. Rev. D* **85** (2012) 055007 [[1110.4625](#)].
- [86] S. Kanemura and K. Yagyu, *Radiative corrections to electroweak parameters in the Higgs triplet model and implication with the recent Higgs boson searches*, *Phys. Rev. D* **85** (2012) 115009 [[1201.6287](#)].
- [87] C.-W. Chiang and K. Yagyu, *Testing the custodial symmetry in the Higgs sector of the Georgi-Machacek model*, *JHEP* **01** (2013) 026 [[1211.2658](#)].
- [88] M. Aoki, S. Kanemura, M. Kikuchi and K. Yagyu, *Radiative corrections to the Higgs boson couplings in the triplet model*, *Phys. Rev. D* **87** (2013) 015012 [[1211.6029](#)].
- [89] C. Englert, E. Re and M. Spannowsky, *Triplet Higgs boson collider phenomenology after the LHC*, *Phys. Rev. D* **87** (2013) 095014 [[1302.6505](#)].
- [90] C. Englert, A. Freitas, M.M. Mühlleitner, T. Plehn, M. Rauch, M. Spira et al., *Precision Measurements of Higgs Couplings: Implications for New Physics Scales*, *J. Phys. G* **41** (2014) 113001 [[1403.7191](#)].
- [91] K. Hartling, K. Kumar and H.E. Logan, *The decoupling limit in the Georgi-Machacek model*, *Phys. Rev. D* **90** (2014) 015007 [[1404.2640](#)].
- [92] M. Garcia-Pepin, S. Gori, M. Quiros, R. Vega, R. Vega-Morales and T.-T. Yu, *Supersymmetric Custodial Higgs Triplets and the Breaking of Universality*, *Phys. Rev. D* **91** (2015) 015016 [[1409.5737](#)].
- [93] K. Hartling, K. Kumar and H.E. Logan, *Indirect constraints on the Georgi-Machacek model and implications for Higgs boson couplings*, *Phys. Rev. D* **91** (2015) 015013 [[1410.5538](#)].
- [94] C.-W. Chiang, A.-L. Kuo and T. Yamada, *Searches of exotic Higgs bosons in general mass spectra of the Georgi-Machacek model at the LHC*, *JHEP* **01** (2016) 120 [[1511.00865](#)].
- [95] C.-W. Chiang, A.-L. Kuo and K. Yagyu, *One-loop renormalized Higgs boson vertices in the Georgi-Machacek model*, *Phys. Rev. D* **98** (2018) 013008 [[1804.02633](#)].
- [96] C.-W. Chiang, G. Cottin and O. Eberhardt, *Global fits in the Georgi-Machacek model*, *Phys. Rev. D* **99** (2019) 015001 [[1807.10660](#)].
- [97] A. Banerjee, G. Bhattacharyya and N. Kumar, *Impact of Yukawa-like dimension-five operators on the Georgi-Machacek model*, *Phys. Rev. D* **99** (2019) 035028 [[1901.01725](#)].
- [98] N. Ghosh, S. Ghosh and I. Saha, *Charged Higgs boson searches in the Georgi-Machacek model at the LHC*, *Phys. Rev. D* **101** (2020) 015029 [[1908.00396](#)].
- [99] C.H. de Lima, D. Stolarski and Y. Wu, *Status of negative coupling modifiers for extended Higgs sectors*, *Phys. Rev. D* **105** (2022) 035019 [[2111.02533](#)].
- [100] A. Kundu, P. Mondal and P.B. Pal, *Custodial symmetry, the Georgi-Machacek model, and other scalar extensions*, *Phys. Rev. D* **105** (2022) 115026 [[2111.14195](#)].
- [101] S. Kanemura and K. Yagyu, *Implication of the W boson mass anomaly at CDF II in the Higgs triplet model with a mass difference*, *Phys. Lett. B* **831** (2022) 137217 [[2204.07511](#)].
- [102] P. Mondal, *Enhancement of the W boson mass in the Georgi-Machacek model*, *Phys. Lett. B* **833** (2022) 137357 [[2204.07844](#)].
- [103] T.-K. Chen, C.-W. Chiang, C.-T. Huang and B.-Q. Lu, *Updated constraints on the Georgi-Machacek model and its electroweak phase transition and associated gravitational waves*, *Phys. Rev. D* **106** (2022) 055019 [[2205.02064](#)].
- [104] R. Ghosh and B. Mukhopadhyaya, *Some new observations for the Georgi-Machacek scenario with triplet Higgs scalars*, *Phys. Rev. D* **107** (2023) 035031 [[2212.11688](#)].

- [105] T.-K. Chen, C.-W. Chiang and K. Yagyu, *CP violation in a model with Higgs triplets*, *JHEP* **06** (2023) 069 [[2303.09294](#)].
- [106] M. Chakraborti, D. Das, N. Ghosh, S. Mukherjee and I. Saha, *New physics implications of vector boson fusion searches exemplified through the Georgi-Machacek model*, *Phys. Rev. D* **109** (2024) 015016 [[2308.02384](#)].
- [107] D. Das, A. Kundu, M. Levy, A.M. Prasad, I. Saha and A. Sarkar, *Sign of the  $hZZ$  coupling and implication for new physics*, *Phys. Lett. B* **857** (2024) 139002 [[2402.09352](#)].
- [108] C.H. de Lima and D. Stolarski, *Influence of new states in searches for negative gauge-Higgs couplings*, *JHEP* **10** (2024) 180 [[2404.10815](#)].
- [109] A. Crivellin, S. Ashanujjaman, S. Banik, G. Coloretti, S.P. Maharathy and B. Mellado, *Growing evidence for a Higgs triplet\**, *Chin. Phys. C* **49** (2025) 053107 [[2404.14492](#)].
- [110] D. Chowdhury, P. Mondal and S. Samanta, *Next-to-Leading Order Unitarity Fits in the Extended Georgi-Machacek Model*, [2404.18996](#).
- [111] C.-T. Lu, X. Wang, X. Wei and Y. Wu, *Probing long-lived doubly charged scalar in the Georgi-Machacek model at the LHC and in far detectors*, *JHEP* **02** (2025) 149 [[2410.19561](#)].
- [112] L. Shang, Y. Wang, X. Du, B. Yang and S. Moretti, *Tripletino-like WIMP Dark Matter in the Supersymmetric Georgi-Machacek Model*, [2503.02653](#).
- [113] C.-T. Lu, Y. Wu and S. Xu, *Dark Matter and Electroweak Phase Transition in the  $Z_2$  Symmetric Georgi-Machacek Model*, [2504.10930](#).
- [114] C. Henderson, *Future Physics Prospects with the CMS Detector at the High-Luminosity LHC*, *SciPost Phys. Proc.* (2022) 111.
- [115] W. Bizoń, U. Haisch, L. Rottoli, Z. Gillis, B. Moser and P. Windischhofer, *Addendum to: Constraints on the quartic Higgs self-coupling from double-Higgs production at future hadron colliders [*JHEP* 10 (2019) 267]*, *JHEP* **02** (2024) 170 [[2402.03463](#)].
- [116] P. Stylianou and G. Weiglein, *Constraints on the trilinear and quartic Higgs couplings from triple Higgs production at the LHC and beyond*, *Eur. Phys. J. C* **84** (2024) 366 [[2312.04646](#)].
- [117] J.M. Torndal, J. List, D. Ntounis and C. Vernieri, *Higgs self-coupling measurement at future  $e^+e^-$  colliders*, *PoS EPS-HEP2023* (2024) 406 [[2311.16774](#)].
- [118] E. Celada, T. Giani, J. ter Hoeve, L. Mantani, J. Rojo, A.N. Rossia et al., *Mapping the SMEFT at High-Energy Colliders: from LEP and the (HL-)LHC to the FCC-ee*, [2404.12809](#).
- [119] C. Aime et al., *Muon Collider Physics Summary*, [2203.07256](#).
- [120] MUON COLLIDER collaboration, *The physics case of a 3 TeV muon collider stage*, [2203.07261](#).
- [121] M. Forsslund and P. Meade, *High precision higgs from high energy muon colliders*, *JHEP* **08** (2022) 185 [[2203.09425](#)].
- [122] S. Bhattacharyya, B. Bhattacharjee, C. Bose, D. Chowdhury and S. Mukherjee, *Tagging ultra-boosted jets at FCC-hh using machine learning techniques*, [2501.06702](#).
- [123] LINEAR COLLIDER VISION collaboration, *A Linear Collider Vision for the Future of Particle Physics*, [2503.19983](#).
- [124] HFLAV collaboration, *Averages of  $b$ -hadron,  $c$ -hadron, and  $\tau$ -lepton properties as of 2021*, *Phys. Rev. D* **107** (2023) 052008 [[2206.07501](#)].
- [125] J.L. Hewett, *Can  $b \rightarrow s$  gamma close the supersymmetric Higgs production window?*, *Phys. Rev. Lett.* **70** (1993) 1045 [[hep-ph/9211256](#)].
- [126] V.D. Barger, M.S. Berger and R.J.N. Phillips, *Implications of  $b \rightarrow s$  gamma decay measurements in testing the MSSM Higgs sector*, *Phys. Rev. Lett.* **70** (1993) 1368 [[hep-ph/9211260](#)].
- [127] A.J. Buras, M. Misiak, M. Munz and S. Pokorski, *Theoretical uncertainties and phenomenological aspects of  $B \rightarrow X(s)$  gamma decay*, *Nucl. Phys. B* **424** (1994) 374 [[hep-ph/9311345](#)].
- [128] G.C. Branco, P.M. Ferreira, L. Lavoura, M.N. Rebelo, M. Sher and J.P. Silva, *Theory and phenomenology of two-Higgs-doublet models*, *Phys. Rept.* **516** (2012) 1 [[1106.0034](#)].
- [129] T. Hermann, M. Misiak and M. Steinhauser,  *$\bar{B} \rightarrow X_s \gamma$  in the Two Higgs Doublet Model up to Next-to-Next-to-Leading Order in QCD*, *JHEP* **11** (2012) 036 [[1208.2788](#)].
- [130] M. Misiak, A. Rehman and M. Steinhauser, *Towards  $\bar{B} \rightarrow X_s \gamma$  at the NNLO in QCD without interpolation in  $m_c$* , *JHEP* **06** (2020) 175 [[2002.01548](#)].
- [131] M. Misiak et al., *Updated NNLO QCD predictions for the weak radiative  $B$ -meson decays*, *Phys. Rev. Lett.* **114** (2015) 221801 [[1503.01789](#)].



- [132] M. Czakon, P. Fiedler, T. Huber, M. Misiak, T. Schutzmeier and M. Steinhauser, *The  $(Q_7, Q_{1,2})$  contribution to  $\bar{B} \rightarrow X_s \gamma$  at  $\mathcal{O}(\alpha_s^2)$* , *JHEP* **04** (2015) 168 [[1503.01791](#)].
- [133] M. Misiak and M. Steinhauser, *Weak radiative decays of the  $B$  meson and bounds on  $M_{H^\pm}$  in the Two-Higgs-Doublet Model*, *Eur. Phys. J. C* **77** (2017) 201 [[1702.04571](#)].
- [134] M. Misiak and M. Steinhauser, *NNLO QCD corrections to the anti- $B \rightarrow X(s)$  gamma matrix elements using interpolation in  $m(c)$* , *Nucl. Phys. B* **764** (2007) 62 [[hep-ph/0609241](#)].
- [135] M. Misiak et al., *Estimate of  $\mathcal{B}(\bar{B} \rightarrow X_s \gamma)$  at  $\mathcal{O}(\alpha_s^2)$* , *Phys. Rev. Lett.* **98** (2007) 022002 [[hep-ph/0609232](#)].
- [136] A. Gunawardana and G. Paz, *Reevaluating uncertainties in  $\bar{B} \rightarrow X_s \gamma$  decay*, *JHEP* **11** (2019) 141 [[1908.02812](#)].
- [137] M. Ciuchini, G. Degrandi, P. Gambino and G.F. Giudice, *Next-to-leading QCD corrections to  $B \rightarrow X_s \gamma$ : Standard model and two Higgs doublet model*, *Nucl. Phys. B* **527** (1998) 21 [[hep-ph/9710335](#)].
- [138] K.G. Chetyrkin, M. Misiak and M. Munz, *Weak radiative  $B$  meson decay beyond leading logarithms*, *Phys. Lett. B* **400** (1997) 206 [[hep-ph/9612313](#)].
- [139] W.-S. Hou and R.S. Willey, *Effects of Charged Higgs Bosons on the Processes  $b \rightarrow s$  Gamma,  $b \rightarrow s g^*$  and  $b \rightarrow s$  Lepton+ Lepton-*, *Phys. Lett. B* **202** (1988) 591.
- [140] B. Grinstein, R.P. Springer and M.B. Wise, *Strong Interaction Effects in Weak Radiative  $\bar{B}$  Meson Decay*, *Nucl. Phys. B* **339** (1990) 269.
- [141] D. Chowdhury and O. Eberhardt, *Update of Global Two-Higgs-Doublet Model Fits*, *JHEP* **05** (2018) 161 [[1711.02095](#)].
- [142] ATLAS collaboration, *ATLAS searches for additional scalars and exotic Higgs boson decays with the LHC Run 2 dataset*, [2405.04914](#).
- [143] J. De Blas et al., *HEPfit: a code for the combination of indirect and direct constraints on high energy physics models*, *Eur. Phys. J. C* **80** (2020) 456 [[1910.14012](#)].
- [144] A. Caldwell, D. Kollar and K. Kroninger, *BAT: The Bayesian Analysis Toolkit*, *Comput. Phys. Commun.* **180** (2009) 2197 [[0808.2552](#)].
- [145] J. de Blas, M. Ciuchini, E. Franco, S. Mishima, M. Pierini, L. Reina et al., *Electroweak precision observables and Higgs-boson signal strengths in the Standard Model and beyond: present and future*, *JHEP* **12** (2016) 135 [[1608.01509](#)].
- [146] LEP HIGGS WORKING GROUP FOR HIGGS BOSON SEARCHES, ALEPH, DELPHI, L3, OPAL collaboration, *Search for charged Higgs bosons: Preliminary combined results using LEP data collected at energies up to 209-GeV*, in *2001 Europhysics Conference on High Energy Physics*, 7, 2001 [[hep-ex/0107031](#)].
- [147] ATLAS collaboration, *Evidence of off-shell Higgs boson production from ZZ leptonic decay channels and constraints on its total width with the ATLAS detector*, *Phys. Lett. B* **846** (2023) 138223 [[2304.01532](#)].
- [148] CMS collaboration, *Measurement of the Ratio  $\mathcal{B}(t \rightarrow Wb)/\mathcal{B}(t \rightarrow Wq)$  in  $pp$  Collisions at  $\sqrt{s} = 8$  TeV*, *Phys. Lett. B* **736** (2014) 33 [[1404.2292](#)].
- [149] V. Cacchio, D. Chowdhury, O. Eberhardt and C.W. Murphy, *Next-to-leading order unitarity fits in Two-Higgs-Doublet models with soft  $\mathbb{Z}_2$  breaking*, *JHEP* **11** (2016) 026 [[1609.01290](#)].
- [150] A.M. Coutinho, A. Karan, V. Miralles and A. Pich, *Light scalars within the CP-conserving Aligned-two-Higgs-doublet model*, *JHEP* **02** (2025) 057 [[2412.14906](#)].
- [151] A. Djouadi, J. Kalinowski and P.M. Zerwas, *Two and three-body decay modes of SUSY Higgs particles*, *Z. Phys. C* **70** (1996) 435 [[hep-ph/9511342](#)].
- [152] CMS collaboration, *A Search for a Doubly-Charged Higgs Boson in  $pp$  Collisions at  $\sqrt{s} = 7$  TeV*, *Eur. Phys. J. C* **72** (2012) 2189 [[1207.2666](#)].
- [153] ATLAS collaboration, *Search for anomalous production of prompt same-sign lepton pairs and pair-produced doubly charged Higgs bosons with  $\sqrt{s} = 8$  TeV  $pp$  collisions using the ATLAS detector*, *JHEP* **03** (2015) 041 [[1412.0237](#)].
- [154] CMS collaboration, *A search for doubly-charged Higgs boson production in three and four lepton final states at  $\sqrt{s} = 13$  TeV*, .
- [155] ATLAS collaboration, *Combination of searches for singly and doubly charged Higgs bosons produced via vector-boson fusion in proton-proton collisions at  $\sqrt{s} = 13$  TeV with the ATLAS detector*, *Phys. Lett. B* **860** (2025) 139137 [[2407.10798](#)].

- [156] ATLAS collaboration, *Search for charged Higgs bosons decaying via  $H^\pm \rightarrow \tau^\pm \nu$  in fully hadronic final states using  $pp$  collision data at  $\sqrt{s} = 8$  TeV with the ATLAS detector*, *JHEP* **03** (2015) 088 [[1412.6663](#)].
- [157] CMS collaboration, *Search for a charged Higgs boson in  $pp$  collisions at  $\sqrt{s} = 8$  TeV*, *JHEP* **11** (2015) 018 [[1508.07774](#)].
- [158] ATLAS collaboration, *Search for charged Higgs bosons decaying via  $H^\pm \rightarrow \tau^\pm \nu_\tau$  in the  $\tau$ +jets and  $\tau$ +lepton final states with  $36 \text{ fb}^{-1}$  of  $pp$  collision data recorded at  $\sqrt{s} = 13$  TeV with the ATLAS experiment*, *JHEP* **09** (2018) 139 [[1807.07915](#)].
- [159] CMS collaboration, *Search for charged Higgs bosons in the  $H^\pm \rightarrow \tau^\pm \nu_\tau$  decay channel in proton-proton collisions at  $\sqrt{s} = 13$  TeV*, *JHEP* **07** (2019) 142 [[1903.04560](#)].
- [160] CMS collaboration, *Search for charged Higgs bosons decaying into a top and a bottom quark in the all-jet final state of  $pp$  collisions at  $\sqrt{s} = 13$  TeV*, *JHEP* **07** (2020) 126 [[2001.07763](#)].
- [161] ATLAS collaboration, *Search for charged Higgs bosons decaying into a top quark and a bottom quark at  $\sqrt{s} = 13$  TeV with the ATLAS detector*, *JHEP* **06** (2021) 145 [[2102.10076](#)].
- [162] ATLAS collaboration, *Search for charged Higgs bosons in the  $H^\pm \rightarrow tb$  decay channel in  $pp$  collisions at  $\sqrt{s} = 8$  TeV using the ATLAS detector*, *JHEP* **03** (2016) 127 [[1512.03704](#)].
- [163] ATLAS collaboration, *Search for a Charged Higgs Boson Produced in the Vector-Boson Fusion Mode with Decay  $H^\pm \rightarrow W^\pm Z$  using  $pp$  Collisions at  $\sqrt{s} = 8$  TeV with the ATLAS Experiment*, *Phys. Rev. Lett.* **114** (2015) 231801 [[1503.04233](#)].
- [164] CMS collaboration, *Study of vector boson scattering and search for new physics in events with two same-sign leptons and two jets*, *Phys. Rev. Lett.* **114** (2015) 051801 [[1410.6315](#)].
- [165] ATLAS collaboration, *Search for doubly and singly charged Higgs bosons decaying into vector bosons in multi-lepton final states with the ATLAS detector using proton-proton collisions at  $\sqrt{s} = 13$  TeV*, *JHEP* **06** (2021) 146 [[2101.11961](#)].
- [166] CMS collaboration, *Search for a scalar or pseudoscalar dilepton resonance produced in association with a massive vector boson or top quark-antiquark pair in multilepton events at  $s=13$  TeV*, *Phys. Rev. D* **110** (2024) 012013 [[2402.11098](#)].